Physics of the Earth and Planetary Interiors 224 (2013) 104–123

Contents lists available at ScienceDirect

Physics of the Earth and Planetary Interiors

journal homepage: www.elsevier.com/locate/pepi

Review

Seismic imaging of the deep structure under the Chinese volcanoes: An overview

Jianshe Lei [a,*], Furen Xie [a], Qicheng Fan [b], M. Santosh [c]

[a] Key Laboratory of Crustal Dynamics, Institute of Crustal Dynamics, China Earthquake Administration, Beijing 100085, China
[b] Institute of Geology, China Earthquake Administration, Beijing 100029, China
[c] School of Earth Sciences and Resources, China University of Geosciences, Beijing 100083, China

ARTICLE INFO

Article history:
Received 1 March 2013
Received in revised form 6 August 2013
Accepted 21 August 2013
Available online 30 August 2013
Edited by G. Helffrich

Keywords:
Seismic tomography
Seismic structure
Upper mantle
Volcano
Chinese continent

ABSTRACT

The rapid development of provincial seismic networks and portable seismic arrays has provided a good opportunity to image the detailed 3-D seismic structure of the upper mantle under the active volcanoes in the Chinese continent. Under the Changbaishan (Tianchi) volcano prominent low-velocity (low-V) anomalies are imaged above 400 km depth, and high-velocity (high-V) anomalies are detected within the mantle transition zone, suggesting that the Changbaishan volcano is a back-arc volcano related to the dehydration of the subducted Pacific slab that is stagnant in the mantle transition zone. Seismic structures under the Tengchong volcano are similar to those under the Changbaishan volcano, whereas the subducted slab under the Tengchong volcano is the continental Indian slab. Regional and global tomographic models illustrate that obvious low-V anomalies are visible under the Hainan volcano from the crust down to the lower mantle, suggesting that the Hainan volcano is a hotspot. A recent local tomographic model shows that the Hainan plume is imaged as a southeast tilted low-V anomaly with depth in the upper mantle. A high-resolution upper-mantle tomographic model under the North China Craton shows a significantly Y-shaped low-V anomaly under the Datong volcano and Bohai Sea extending down to the lower mantle, which, for the first time, is inferred using precise teleseismic arrival times hand-picked from high-quality seismograms recorded at densely spaced stations from the Chinese provincial networks. The results indicate the possibility of a mantle plume beneath the region. These models suggest that the Changbaishan and Tengchong volcanoes share the history of deep mantle origin, whereas the Datong and Hainan volcanoes are comparable. All these results provide a better understanding of the dynamics of East Asia, and also call for future volcanic hazard mitigation.

Contents

1. Introduction . . . 105
2. Deep structures under the volcanoes . . . 106
   2.1. The Changbaishan (Tianchi) volcano . . . 106
   2.2. The Tengchong volcano . . . 109
   2.3. The Hainan volcano . . . 113
   2.4. The Datong volcano . . . 114
   2.5. The Xing'an-Mongolia volcanic group . . . 116
3. Discussion . . . 117
   3.1. Seismic tomography with integrated data . . . 117
   3.2. Seismic tomography with later phases . . . 118
   3.3. Ray-theory tomography versus finite-frequency tomography . . . 118
   3.4. Anisotropic tomography . . . 118
   3.5. Future work . . . 119

* Corresponding author. Tel./fax: +86 10 62846760.
E-mail addresses: leijs@eq-icd.cn, jshlei_cj@hotmail.com (J. Lei).

0031-9201
http://dx.doi.org/10.1016/j.pepi.2013.08.008

4. Summary . . . 119
Acknowledgements . . . 119
References . . . 119

1. Introduction

The complex tectonic architecture of East Asia includes the growing Tibetan plateau and Tianshan mountains, the stable Sichuan and Tarim basins, and the lithospheric erosion beneath the North China Craton (Fig. 1). These features have been correlated to the collision of the Indian and Eurasian plates to the southwest (e.g., Molnar and Tapponnier, 1975; England and Houseman, 1986; Tapponnier et al., 1986; Yin and Harrison, 2000; Liu et al., 2004; Guo and Wilson, 2012) and the subduction of the Philippine Sea and Pacific plates to the east (e.g., Fukao et al., 1992; Bijwaard et al., 1998; Zhao, 2004; Abdelwahed and Zhao, 2007; Lei and Zhao, 2005, 2006a; Li and van der Hilst, 2010; Zhao et al., 2012a). Along these tectonic boundaries are distributed many large and active faults and rifts, such as the Tanlu fault and Shanxi rift in eastern China, and the Kunlunshan fault, Xianshui River fault, the Longmenshan fault zones, and the Red-River fault in western China (Fig. 1) (Deng et al., 2002). In addition, around these fault zones some large earthquakes occurred historically and recently. Some well-known examples are the 25 September 1303 Hongtong, Shanxi, earthquake (M 8.0), the 2 February 1556 Huaxian, Shaanxi earthquake (M 8.25), the 14 November 2001 Kunlun earthquake (M 8.1), the 12 May 2008 Wenchuan earthquake (M 8.0), and the 14 April 2010 Yushu earthquake (M 7.1) (Song et al., 2011). These destructive earthquakes caused immense damage to life and property.

Active volcanoes pose another form of serious natural disasters in the Chinese continent (Fig. 1). Volcanoes act as the vents for extremely high-temperature magma ascending upward from the mantle through the crust to the surface. Volcanoes are defined as active if they were recorded at least one eruption in the Holocene. Accord-

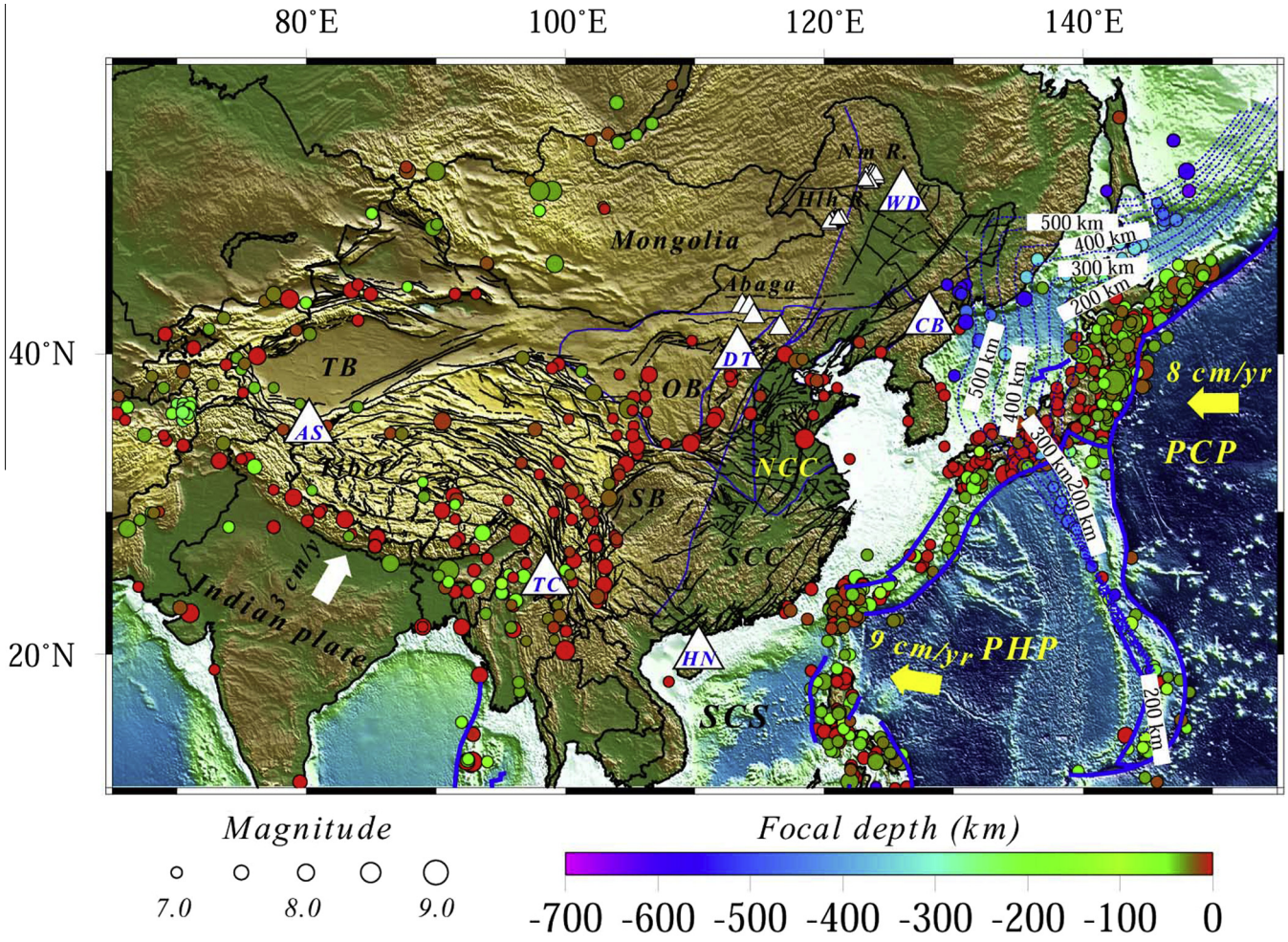

Fig. 1. Distribution of volcanoes (large triangles with letters) in China underlain by topography. WD, the Wudalianchi volcano; CB, the Changbaishan volcano; DT, the Datong volcano; TC, the Tengchong volcano; HN, the Hainan volcano; AS, the Ashikule (Kunlun) volcano. Small triangles denote the volcanoes along the Xing'an-Mongolia orogenic belt. Abaga, the Abaga volcanic group; Hlh R., the Halaha River volcanic group; Nm R., the Nuomin River volcanic group. The NS oriented blue line denotes the North–South Gravity Lineament. Color circles denotes the earthquakes with magnitude larger than 7.0 since BC 780 (Song et al., 2011). The scales for earthquake magnitude and focal depth are shown at the bottom. NCC, the North China Craton; SCC, the South China Craton; SB, the Sichuan basin; OB, the Ordos block; TB, the Tarim basin; PCP, the Pacific plate; PHP, the Philippine Sea plate; SCS, the South China Sea; Thick arrows denote the directions of absolute plate motion, and their velocities are shown on the side of the arrows. Dashed lines denote depth contours of the upper boundary of the subducted Pacific slab (Gudmundsson and Sambridge, 1998). Thick blue lines denote major plate boundaries. Thin black lines denote the major active faults (Deng et al., 2002).

ingly, among the volcanoes in Mainland China, the Wudalianchi, Changbaishan (Tianchi), Tengchong, and Hainan volcanoes are considered to be active (Fig. 1) (Liu, 1999, 2000). Recent petrological studies have demonstrated that there are several groups of active volcanoes in the region, such as the Abaga, the Halaha river, and the Nuomin river groups, from the southwest to the northeast along the Xing'an-Mongolia orogenic belt (Fig. 1), with magma eruption during the Holocene and well-preserved vents (Fig. 2) (e.g., Bai et al., 2005, 2008; Fan et al., 2011, 2012; Chen et al., 2012b).

Volcanic eruptions cause tremendous disasters, because one tenth of the world population lives in volcanically active areas. For instance, the Tambora volcanic eruption in Indonesia killed 92,000 people in 1815. The Ruiz volcanic eruption in Colombia caused about 23,000 deaths in 1985 due to the largest debris flow in the history (Fan, 2005). The Changbaishan volcano is considered to be the most potentially dangerous volcano in China. Within 50 km off the Changbaishan volcanic crater, the number of earthquakes ($M > 1.0$) increased significantly to 72 per month in 2002–2006 from 7 per month in 1999–2002 and 2006–2011, and the most active seismicity occurred in November 2003 with 243 events (Xu et al., 2012c). Portable seismic observations from 2002 to 2003 showed that the small crustal earthquakes become shallower with time under the Changbaishan volcanic crater, and the first-motions go upward on the seismograms recorded at most stations from deep earthquakes (Wu et al., 2005, 2007). These results strongly suggest that the magma chamber beneath the Changbaishan volcano has woken up and resumed its activity since AD 1903. The recent Tohoku-Oki earthquake (M 9.0) which occurred on 11 March 2011 in Northeast Japan was caused by the active subduction of the Pacific slab beneath the Okhotsk plate (Kato and Yoshida, 2011; Zhao et al., 2011a), and the deep subducted Pacific plate has reached under the Changbaishan volcano (Zhao, 2004; Lei and Zhao, 2005, 2006a; Huang and Zhao, 2006; Zhao et al., 2009a; Li and van der Hilst, 2010). Therefore, the Tohoku-Oki earthquake may also impact the mantle dynamics beneath the Changbaishan volcano. The millennium eruption of the Changbaishan volcano destroyed the forest with an area of over 5,000 km^2 around the crater (Liu et al., 1998), and another activity might result in the death of hundred thousand residents within a radius of 100 km from the crater. Wei et al. (2013) also suggested a possible future eruption. Therefore, it is of great significance to investigate the deep seismic structure under the volcanoes in China in order to better understand the deep origins of the volcanoes to mitigate the hazards.

Seismic tomography is a powerful tool to investigate the deep structure under the volcanoes. With the recently rapid development of Chinese provincial seismic networks (Zheng et al., 2009, 2010) and some portable seismic arrays (Hetland et al., 2004; Duan et al., 2009; Lei et al., 2012b) around the volcanoes, it has become possible to image the detailed 3-D velocity structure under some of these volcanoes, where seismic stations are densely spaced. In this overview, we synthesize the results from the deep seismic images of the upper mantle under the Changbaishan, Tengchong, Hainan volcanoes as well as the Datong volcano (Fig. 1). We also evaluate the advantages of recently updated seismic tomographic techniques for deriving potential information. This work updates a previous review of Zhao and Liu (2010) on this topic, with more detailed synthesis of all the available information.

2. Deep structures under the volcanoes

2.1. The Changbaishan (Tianchi) volcano

The Changbaishan (Tianchi) volcano, also termed as the Baitoushan volcano, is located in the Changbaishan mountains, close to the boundary between NE China and North Korea (Fig. 1). This volcano erupted six times in BC 1120, AD 1050, 1413, 1597, 1668, and 1702 (Simkin and Siebert, 1994). The history of this volcano and the resultant picturesque-landscape (Fig. 2a) attract many geoscientists worldwide for geological, geochemical and geophysical investigations (e.g., Zhang and Tang, 1983; Zindler and Hart, 1986; Basu et al., 1991; Fan and Hooper, 1991; Tang et al., 1997, 2001; Fan et al., 1998, 1999; Zou et al., 2008, 2010b; Wang et al., 2003b; Li et al., 2012). Magnetotelluric soundings show that low resistivity anomalies exist beneath the Changbaishan volcano in the crust (Tang et al., 1997, 2001). Seismic explosion experiments revealed low-velocity anomalies in the crust and upper mantle down to a depth of 40 km. These results suggest the existence of magma chambers under the Changbaishan volcano (Zhang et al., 2002). These geophysical results are well consistent with petrological observations (e.g., Fan et al., 2001). The Changbaishan volcano is about 1200 km away from the Japan Trench (Fig. 1), and its deep origin is still unclear. Turcotte and Schubert (1982) assumed that it is a hotspot like Hawaii volcano, whereas Tatsumi et al. (1990) attributed a back-arc setting.

Global tomographic models (e.g., Zhao, 2004, 2009; Lei and Zhao, 2006a; Zhao et al., 2013) show prominent high-V anomalies in the mantle transition zone under the Changbaishan volcano and broad low-V anomalies above the mantle transition zone, suggesting that the subducting Pacific slab has reached under the Changbaishan volcano. However, the global models are too generalized to evaluate the detailed structure under the Changbaishan volcano. Therefore, Lei and Zhao (2005) applied the tomographic technique of Zhao et al. (1994) to the relative travel-time residuals recorded at the 19 portable seismic stations as well as 3 permanent seismic stations (MDJ, HIA, and BJT) that are relatively close to these portable seismic stations (Fig. 3A). These portable seismic stations were deployed around the Changbaishan volcano in the Chinese side and were operated from late June to September 1997, ten of which continued till April 1998. In addition, the receiver-function techniques were applied to the data set recorded by the portable seismic network to study the crust and upper mantle discontinuities (Ai et al., 2003; Li and Yuan, 2003; Hetland et al., 2004). These results revealed a thick crust with low-velocity (low-V) anomalies and a thickened mantle transition zone beneath the Changbaishan volcano. From chosen 548 high-quality arrival times in original seismograms recorded from 68 teleseismic events, Lei and Zhao (2005) imaged prominent low-V anomalies of up to −3% with a diameter of about 200 km extending continuously down to 400 km depth (Fig. 3A), the complex geometry of which may reflect the existence of several intraplate volcanoes in the region. The mantle transition zone under the Changbaishan volcano generally exhibits high-velocity (high-V) anomalies (Fig. 3A).

In order to update the tomographic images of Lei and Zhao (2005) under the Changbaishan volcano, some researchers attempted to integrate the seismic data from temporary and permanent seismic stations. For example, Duan et al. (2009) used 1378 relative travel time data recorded at 8 permanent seismic stations and 53 temporary seismic stations from 186 teleseismic events. These temporary seismic stations come from three seismic networks. One is the same seismic network as used by Lei and Zhao (2005). The second was operated during June to September 2002 in and around the Jingpohu volcanic area, comprising 15 broadband seismometers. The third was operated during May 2005 to May 2006 from the Changbaishan to Jingpohu volcanic areas, which consisted of 20 seismic stations. Using the comprehensive dataset, they obtained a new tomographic image which revealed some intermittent low-V anomalies under the Changbaishan volcano in the upper mantle, with some weak (small amplitude) high-V anomalies in the mantle transition zone. Although the model of Duan et al. (2009) has some differences from Lei and Zhao (2005), they show a similar pattern of velocity anomalies.

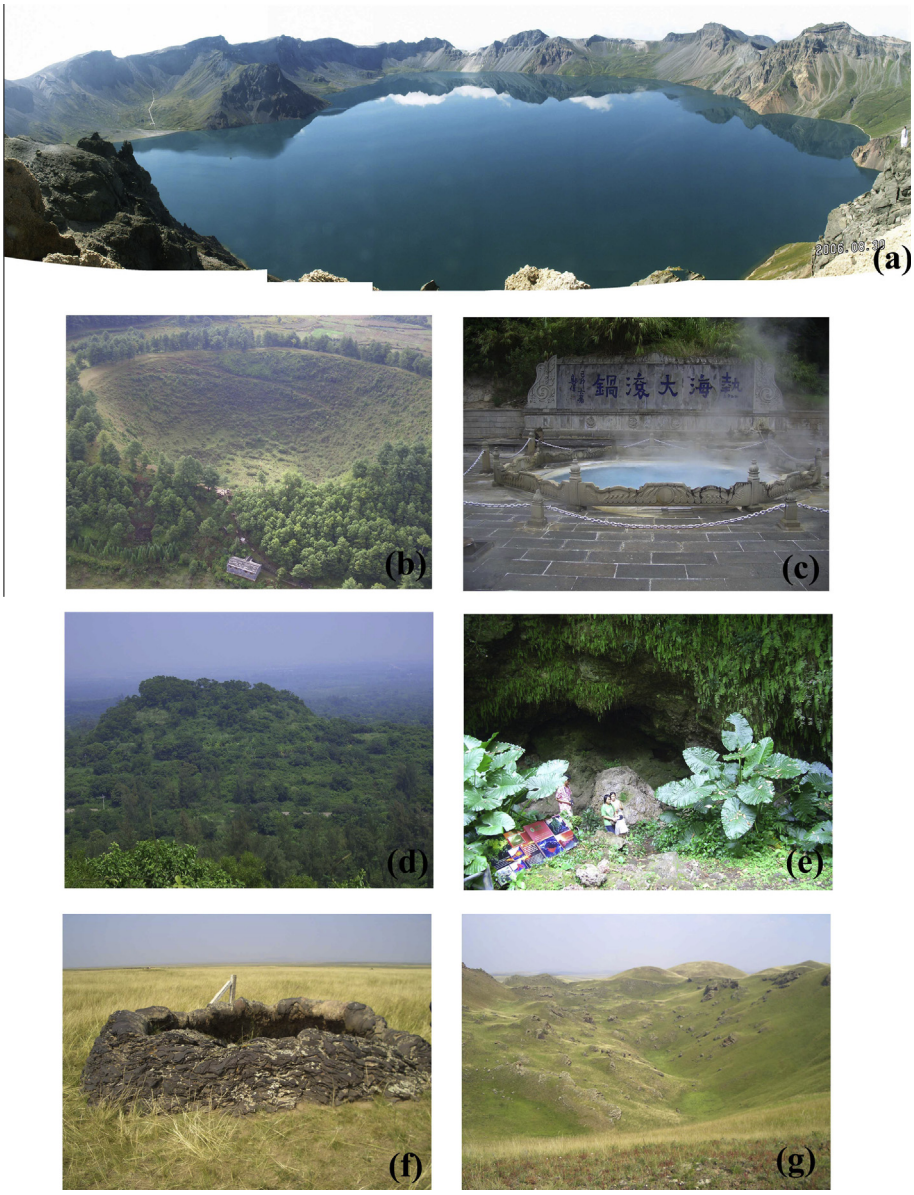

Fig. 2. Photographs of the Changbaishan (Tianchi) (a), and Tengchong (b and c), Hainan (d and e), and Abaga (f and g) volcanoes.

In contrast to Lei and Zhao (2005) and Duan et al. (2009), Zhao et al. (2009a) used a large number of arrival times including relative travel-time residuals from teleseismic events as well as absolute residuals from local and regional events. These data were collected from 19 portable seismic stations as used in the study of Lei and Zhao (2005) and from 645 analog and digital seismic stations of the Chinese provincial seismic networks. The model of Zhao et al. (2009a) (Fig. 3B) shows a similar pattern of velocity anomalies as revealed in previous studies (Fig. 3A) (Lei and Zhao, 2005; Duan et al., 2009), and the results (Fig. 3B) are close to the model of Lei and Zhao (2005). The analysis Zhao et al. (2009a) shows a clear pattern of velocity anomalies, a broad and continuous low-V anomaly under the Changbaishan volcano in the upper mantle and a strong (large amplitude) high-V anomaly in the mantle transition zone (Fig. 3B).

Regional and global tomographic models all show prominent low-V anomalies in the upper mantle and obvious high-V anomalies under the Changbaishan volcano in the mantle transition zone (e.g., Fukao et al., 1992; Bijwaard et al., 1998; Zhao, 2004; Lei and Zhao, 2005, 2006a; Zhao et al., 2009a, 2013) (Fig. 3). The Harvard CMT solutions of deep earthquakes at 200–600 km depths under the Japan sea and East Asia show the compressive stress regime nearly parallel to the down-dip direction of the slab (Ekstrom et al., 2005; Zhao et al., 2009a). The receiver function analyses illustrate a much thick mantle transition zone under the Changbaishan volcano (Ai et al., 2003; Li and Yuan, 2003). All these results suggest that the Pacific slab did not penetrate down the lower mantle directly, but met a strong resistance at the 660-km discontinuity and has been stagnant there for a long time (Maruyama, 1994; Zhao, 2004, 2009).

Tatsumi et al. (1990) first proposed the asthenospheric injection to explain the formation of Changbaishan volcanoes, but they did not mention the stagnant Pacific slab under the region because such a slab was unknown at that time. Lei and Zhao (2005) and Zhao et al. (2007a) modified their model to emphasize the role of the stagnant slab and the big mantle wedge in the formation of intraplate volcanism in Northeastern Asia. This big mantle wedge structure was also supported by recent S-wave splitting (Liu et al., 2008b) and geochemical analysis (Zou et al., 2008). Although Zou et al. (2008) argued against the deep dehydration processes, they suggested that

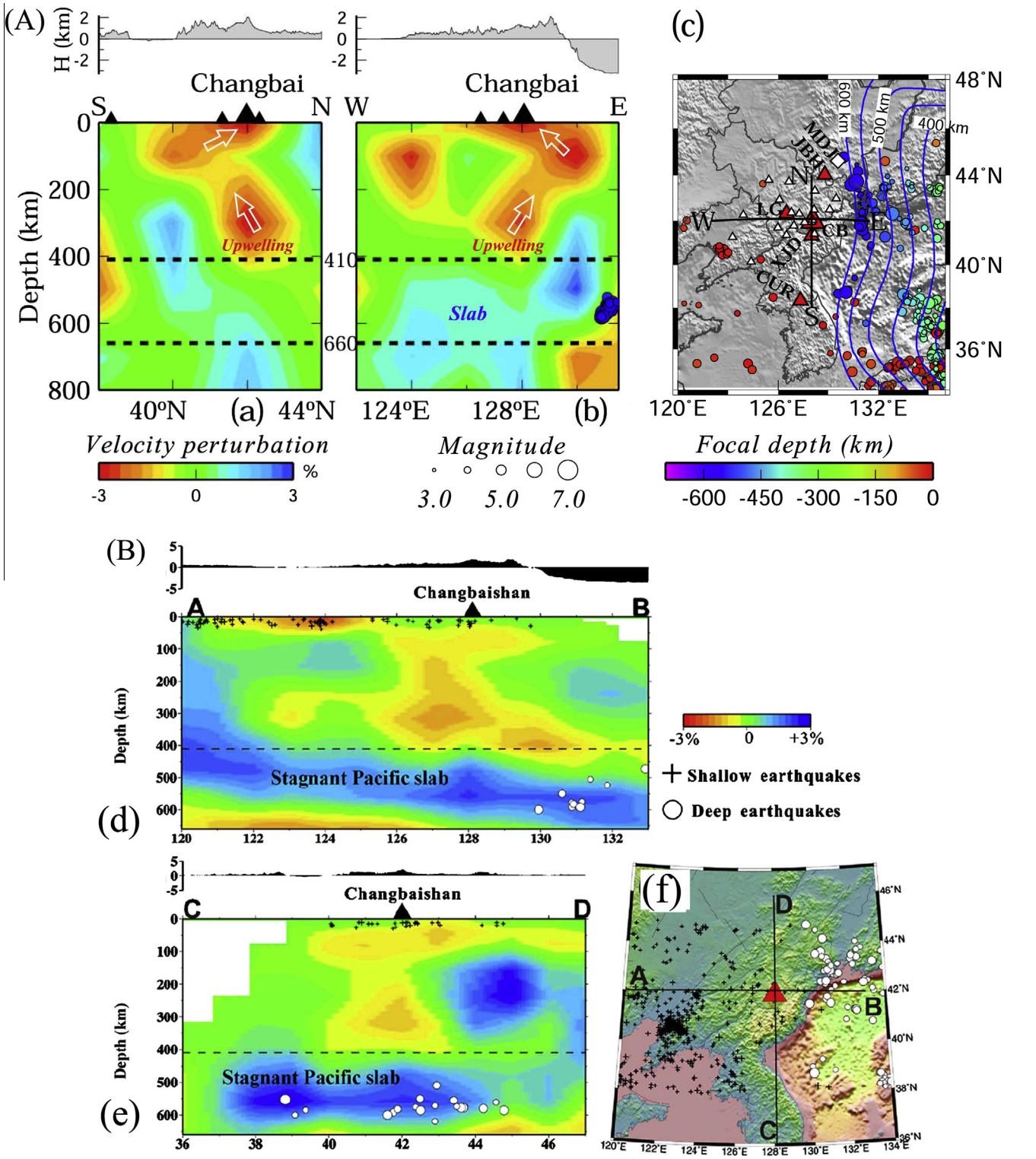

Fig. 3. (A) (a and b) Vertical cross sections of P-wave velocity anomalies (Lei and Zhao, 2005). Red and blue colors denote low-V and high-V anomalies. Velocity perturbations are shown at the bottom. Two dashed lines denote the 410 and 660 km discontinuities. White arrows denote possible directions of hot material upwelling. Color circles denote the earthquakes determined by Engdahl et al. (1998). The scales for magnitude and focal depth are shown at the bottom. Topographies along the cross sections are illustrated on the top. (c) Location of vertical cross-sections (black lines), 19 portable seismic stations (open triangles) and permanent stations (diamonds) used in this study. Solid triangles denote the intraplate volcanoes. CB, Changbaishan; JBH, Jingbohu; LG, Longgang; XJD, Xianjindao; CUR, Ch'Uga-Ryong (Simkin and Siebert, 1994). Dotted lines show depth contours of the Wadati-Benioff deep seismic zone (Gudmundsson and Sambridge, 1998). Modification after Lei and Zhao (2005). (B) (d and e) Tomographic images (Zhao et al., 2009a,b) along vertical cross sections passing through the Changbaishan volcano (CB, a big triangle). Red and blue colors denote low-V and high-V anomalies. The scale for velocity perturbations is shown on the right of (d). Location of cross-sections is shown on the insert map (f).

the piling up and thickening of the stagnant Pacific slab in the mantle transition zone as well as the convection circulation process in the mantle wedge would help drive the asthenosphere upwelling and induce decompression melting. However, a recent estimate of water content and geotherm from electrical conductivity and P-wave velocity in this mantle wedge under northeastern China

showed that neither a dry pyrolite nor a dry harzburgite condition provides consistent electrical and seismic geotherms in the deeper part of the upper mantle (250–400 km depth), but the observed features can be explained by allowing for a small amount of water (500–1000 ppm H/Si) with the seismic geotherm (Ichiki et al., 2006). In the shallower part of the upper mantle (<250 km depth), the electrical and seismic geotherms are consistent with each other within 1500–1700 °C under a dry harzburgite condition, whereas they are not consistent by 100 °C under a dry pyrolite condition (Ichiki et al., 2006). Alternately, if a wet pyrolite condition exists in the deeper part of the upper mantle, the electrical conductivity and seismic P-wave structure can be consistent with each other in the shallower part of the upper mantle (Ichiki et al., 2006). These results suggest the presence of fluids in the entire upper mantle or at least the asthenosphere under northeastern China including the Changbaishan volcanic field, which is consistent with obvious low-V anomalies in the mantle wedge (Fig. 3). This wet upper mantle could be likely caused by the deep stagnancy and dehydration of the subducted Pacific slab in the mantle transition zone (Shieh et al., 1998; Huang et al., 2005; Ohtani et al., 2004; Komabayashi et al., 2004). Seismological studies and numerical models also demonstrate that tens of kilometers thick hydrous layers above the slab carried a considerable amount of water (e.g., ~1 wt% H_2O on the average within the hydrous layer beneath the central Japan) and reached the mantle transition zone (Tonegawa et al., 2008; Iwamori, 2004; Richard and Iwamori, 2010). Because the very old Pacific plate is subducting beneath East Asia at a rapid rate (7–10 cm/year), the dehydration reactions may not completely cease at the shallow depth (100–200 km) of the mantle. Hydrous Mg–Si minerals in the stagnant Pacific slab may continue to release fluids through dehydration reactions in the mantle transition zone (Inoue, 1994; Huang et al., 2005; Ohtani et al., 2004; Komabayashi et al., 2004). Similar dehydration reactions are also observed in the Tonga subduction zone (Zhao et al., 1997; Conder and Wiens, 2006).

Volcanism on the globe are generally of four types: mid-ocean ridge volcanism, subduction zone volcanism, hotspots related to mantle plumes, and intraplate volcanism associated with lithospheric extension and asthenospheric injection (Tatsumi et al., 1990; Yin, 2000; Zhao, 2001). Apparently, the Changbaishan volcanism does not belong to the first type. Because of the stagnant Pacific slab beneath Northeast Asia, the deep origin of Changbaishan volcano differs from that of the Hawaii, Iceland, and Eifel volcanoes which are considered to be related to hotspots overlying the mantle plumes (e.g., Wolfe et al., 1997; Ritsema et al., 1999; Ritter et al., 2001; Zhao, 2001; Lei and Zhao, 2006b). The Changbaishan volcano is located about 1200 km away from Japan Trench, and the subducting Pacific slab has arrived under the volcano in the mantle transition zone. Therefore, Northwestern Pacific subduction zone is considered to be a very broad deformation zone, and the deep subduction of the Pacific slab has influenced the volcanic activity in the interior of the Eurasian continental plate.

All these results further correlate the Changbaishan volcano as a back-arc volcano generated by the hot and wet material upwelling in the big mantle wedge above the stagnant Pacific slab in the mantle transition zone accompanied by slab dehydration (Fig. 4) (Zhao et al., 2004, 2011b; Lei and Zhao, 2005; Zhao and Liu, 2010).

2.2. The Tengchong volcano

The Tengchong volcano in southwest China is located on the southeastern margin of the Tibetan plateau (Fig. 1) with several active faults and large earthquakes recorded around the volcano (Fig. 5a). More recent moderate-strong earthquakes occurred in the region and well-known examples are the 4 February 2011 India-Burma earthquake (M 6.4), the 10 March 2011, Yingjiang, China, earthquake (M 5.8) and the 24 March 2011 Burma earthquake (M 7.2) (Fig. 5). Although the 10 March 2011 Yingjiang earthquake was moderate in size, it caused 25 deaths and 250 injuries, and left numerous people homeless (Lei et al., 2012a, 2012b), perhaps because its focal depth is ~8.3 km (Lei et al., 2012b) and the hypocenter is only 3 km from the center of the Yingjiang county. In particular, to the west, some intermediate-depth earthquakes define a clear Wadati-Benioff deep seismic zone down to ~180 km depth (Fig. 5) (Engdahl et al., 1998). These recent earthquake activities may indicate that the Indian plate is still active and currently subducting eastward, which could affect the Tengchong volcanism (Lei et al., 2012a).

The last eruption of the Tengchong volcano was in 1609, which is similar to that of the 1702 eruption of the Changbaishan volcano (Simkin and Siebert, 1994), but the Tengchong volcanic field is different from the Changbaishan volcanic field. In the Tengchong volcanic field, in addition to picturesque landscapes, numerous

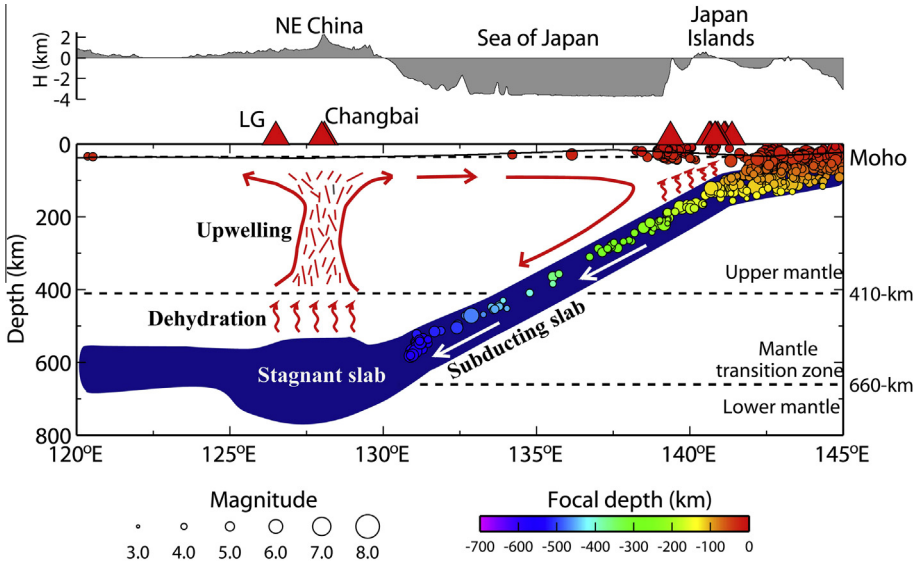

Fig. 4. A schematic east–west vertical section showing the origin of the Changbaishan volcano and intraplate volcanoes in NE Asia (after Tatsumi et al., 1990; Zhao et al., 2004; Lei and Zhao, 2005). LG, the Longgang volcano. Color circles denote the earthquakes determined by Engdahl et al. (1998). These earthquakes and volcanoes are located in the ranges of 41.5°N and 42.5°N. The scales for earthquake magnitude and focal depth are shown at the bottom. Topography along the cross sections is illustrated on the top.

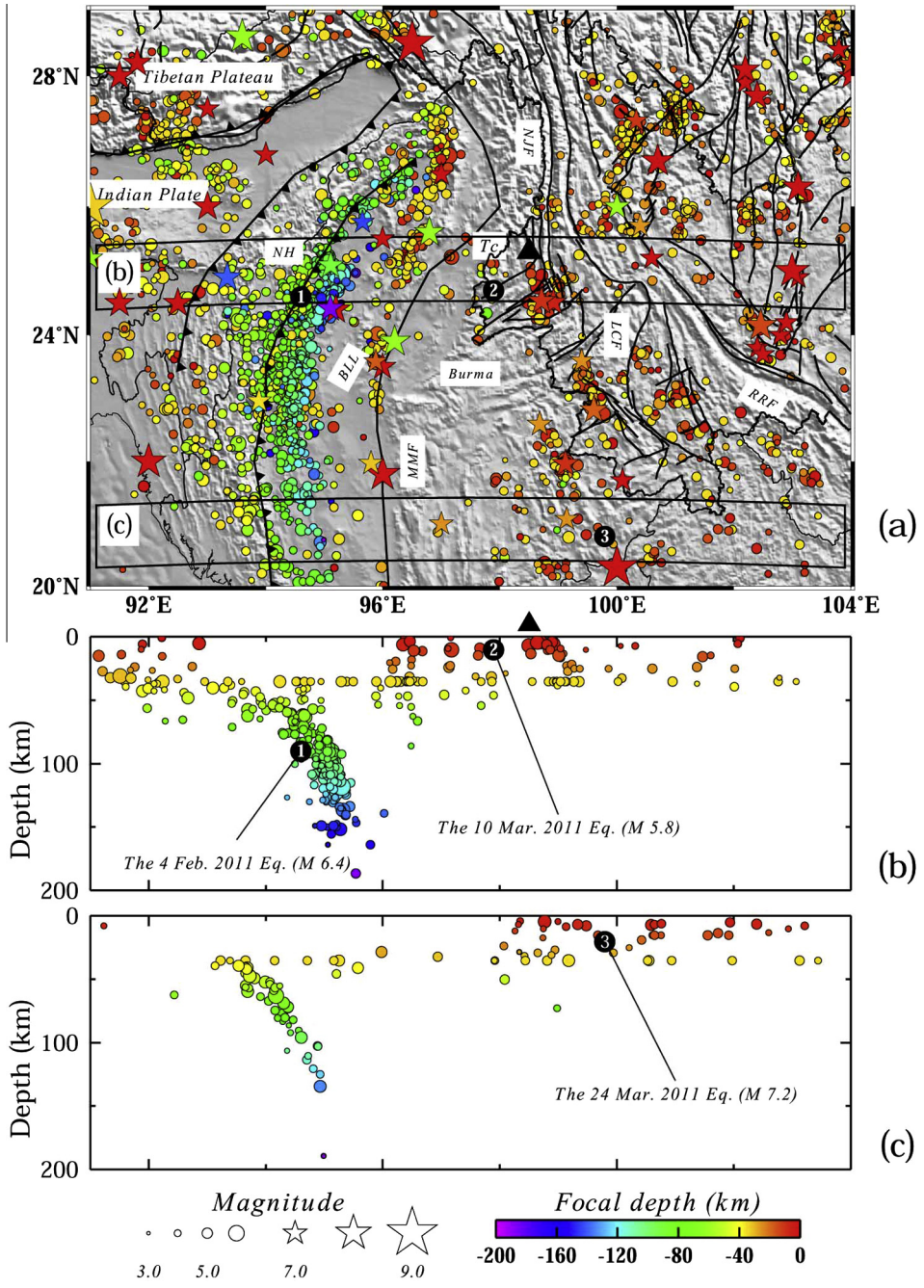

Fig. 5. (a) Location of the Tengchong intraplate volcano (Tc, black triangle) and tectonic settings. Black circles with numbers 1, 2, and 3 denote the 4 February 2011 India-Burma earthquake (*M* 6.4), the 10 March 2011 Yingjiang, China, earthquake (*M* 5.8) and the 24 March 2011 Burma earthquake (*M* 7.2). Black traces denote the major active faults (Deng et al., 2002). Small dots denote earthquakes with magnitude greater than 3.0 (Engdahl et al., 1998), while stars show larger earthquakes with magnitude larger than 6.0. The scales for earthquake magnitude and focal depth are shown at the bottom. Two rectangles represent the two vertical cross section locations in (b and c). NH, Naga Hills; BLL, Burma Lower Lands; MMF, Mandalay-Myityina fault; RRF, Red River fault; NJF, Nujiang fault; LCF, Lancang River fault. (b and c) Vertical cross sections showing the earthquakes within the rectangles as shown in (a). After Lei et al. (2012a).v

hot springs with temperatures of about 90°C also exist (Fig. 2b–c) (Zhao et al., 2006, 2011, 2012c). A gneissic basement with minor amphibolites and rift-related volcanic activity over the last ca. 5 Ma has been identified in the region (Zhu et al., 1983; Yin, 2000; Wang et al., 2001). The Tengchong volcanic field exhibits a high geothermal gradient (Zhao et al., 2006), low seismic velocity in the crust and uppermost mantle (Wang and Huangfu, 2004; Huang and Zhao, 2006; Hu et al., 2008), and high ratio of He^3/He^4 (Shangguan et al., 2000), suggesting the presence of magma chambers and hot material upwelling under the region. Based on carbon isotope analyses of CO_2 and CH_4 collected from hot springs, Zhao et al. (2011) suggested that the temperature of magma chambers could be around ~650–1200 °C. More recent studies identified three He^3/He^4 anomalous areas: Tengchong-Rehai, Qushi, and Wuhe-Puchuan-Xinhua, with the He^3/He^4 ratios of 5.5 Ra, 4.5 Ra, and 2.0 Ra and over 70%, 50%, and 25% of the mantle-derived helium. The He^3/He^4 ratios in the three areas show a gradual increase with time from 1986 to 2006, suggesting the ongoing hot material

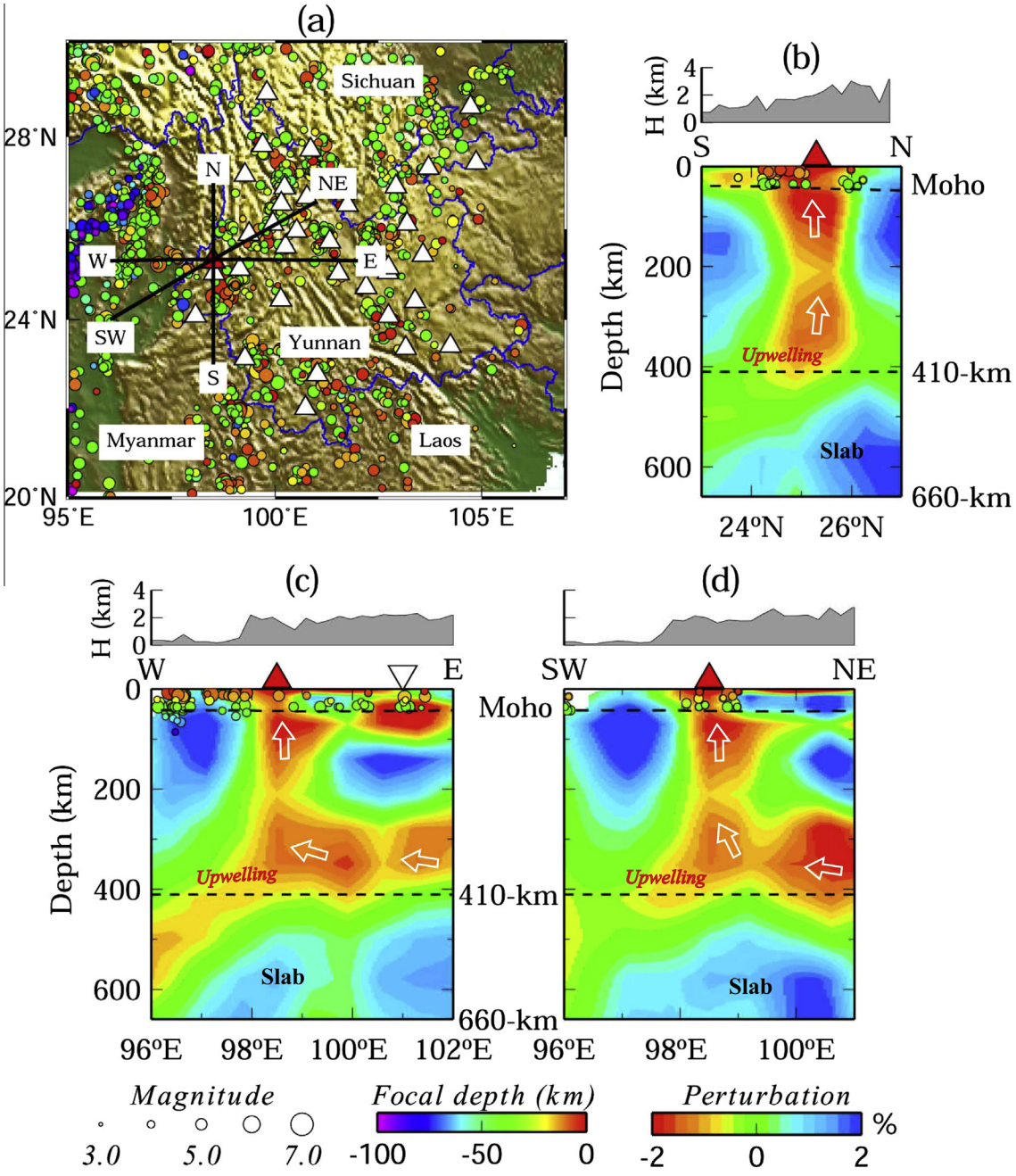

Fig. 6. (a) Locations of three vertical cross-sections (black lines), local earthquakes (circles), and seismic stations (white triangles) used by Lei et al. (2009b). The scales for earthquake magnitude and focal depth are shown at the bottom of (c,d). (b–d) Tomographic images (Lei et al., 2009b) under the Tengchong volcano (red triangle) along these three vertical cross-sections. Red and blue colors denote low-V and high-V anomalies. The scale for velocity perturbations is shown at the bottom of (d). An inverted triangle denotes the Red-River fault. Two dashed lines denote the Moho and 410-km discontinuities. White arrows denote possible directions of hot material upwelling. The topographies along the cross-sections are shown on the top.

upwelling from the mantle which intensifies with time (Zhao et al., 2012c). However, the origin of Tengchong volcano is still debated. Some researchers suggested that the origin of the Tengchong volcano is related to the subduction of the Indian plate down to ~150 km depth (Hu et al., 2008) or even ~200 km depth (Wang and Huangfu, 2004), whereas others ascribed its origin to the subduction of the Burma micro-plate down to depths of 400 km or more (Huang and Zhao, 2006; Li et al., 2008). Global tomographic models provide no useful information on the volcano because of their lower spatial resolution of 300–500 km (e.g., Zhao, 2001, 2004; Lei and Zhao, 2006a). Local tomographic models for this region are valid down to only 80 km depth (e.g., Huang et al., 2002; Wang et al., 2003a).

With the recent upgrading of 35 seismic stations from analogue to digital recording in the Yunnan province, China since 1998, abundant high-quality local and teleseismic data have been accumulated. Lei et al. (2009b) collected 17,190 first P-wave arrival times from 2761 local earthquakes ($M > 2.5$) (Fig. 6a) and hand-picked 11,608 first P-wave arrival times from high-quality seismograms recorded from 602 teleseismic events. Applying the tomographic technique of Zhao et al. (1994) to these arrival times, Lei et al. (2009b) obtained a new tomographic model (Fig. 6b–d).

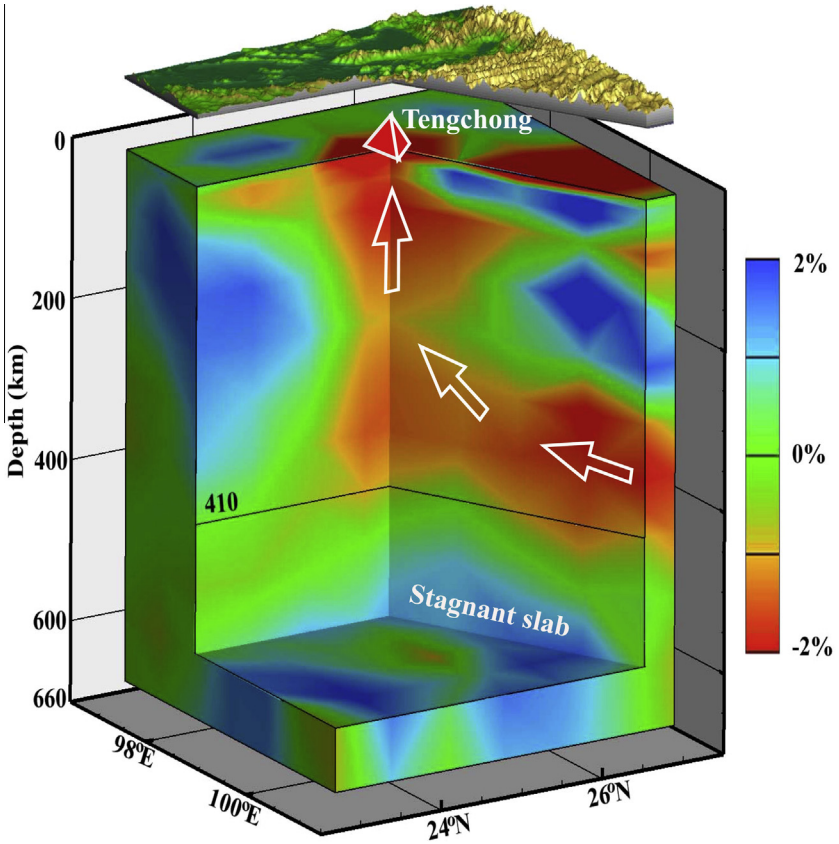

Fig. 7. A 3-D view of tomographic images (Lei et al., 2009b) under the Tengchong volcano (triangle). Red and blue colors denote low-V and high-V anomalies. The scale for velocity perturbation is shown on the right. The topography is shown on the top.

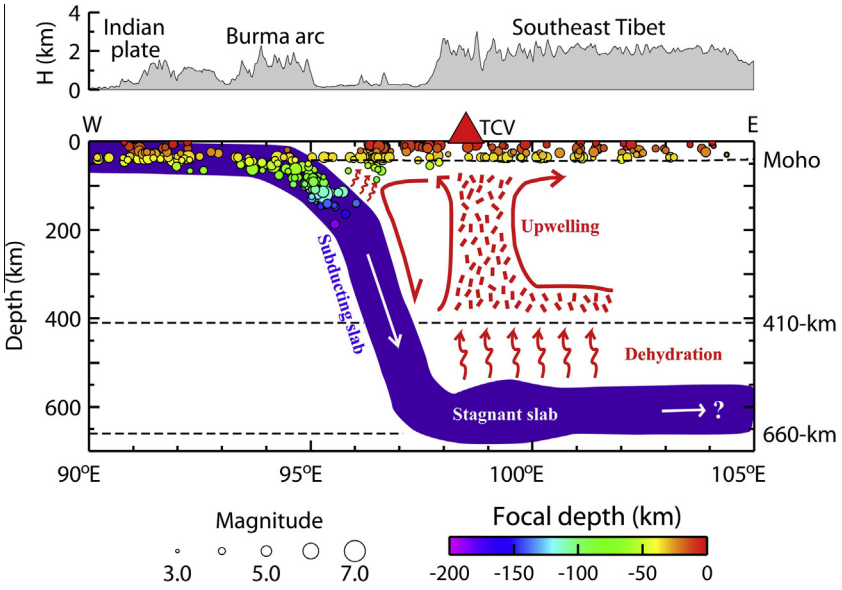

Fig. 8. Schematic tectonic settings showing how to form the Tengchong volcano (TCV, red triangle). The earthquakes determined by Engdahl et al. (1998) are plotted within a range of 35 km off the profile of 25.6°N. The scales for earthquake magnitude and focal depth are shown at the bottom. The topography along the profile is illustrated on the top. After Lei et al. (2009b).

This new model shows a prominent low-V anomaly under the Tengchong volcano extending down to about 400 km depth, and this low-V anomaly spreads horizontally towards the northeast at depths of 250–400 km. High-V anomalies are clearly observed in the mantle transition zone, which could represent the cold subducted Indian slab. To more clearly evaluate the seismic structure

under the Tengchong volcano, a 3-D view is shown in Fig. 7. Li et al. (2008) illustrated high-V anomalies related to the subducted Indian slab down to the mantle transition zone with a steep dip angle of ~60° in the aseismic zone below ~200 km depth. Recent receiver-function analyses demonstrated that the 660-km discontinuity is depressed to 690 km depth under the Tengchong volcano (e.g., Shen et al., 2008). Integrating these results, Lei et al. (2009b) proposed a tectonic model (Fig. 8). The Indian slab has subducted down to the mantle transition zone, though the seismicity within the slab ends at ~200 km depth. The dip angle of the slab varies from ~30° above ~200 km depth in the seismic zone to ~60° below this depth in the aseismic zone, which are quite similar to those observed in the subducted Philippine Sea slab (e.g., Abdelwahed and Zhao, 2007; Zhao et al., 2012a). The eastward subduction of the Indian slab around the Burma arc has also been demonstrated by petrological and geochemical studies (Guo et al., 2005; Zou et al., 2010a; Zhou et al., 2011; Xu et al., 2012a), because the whole rock in the Maanshan (Tengchong) volcanic area is characterized by negative ε_{Nd} (−7.0), high $^{87}Sr/^{86}Sr$ (0.7076) and excess ^{238}U, which may reflect magma generation from an enriched mantle produced by continental subduction (Zou et al., 2010a). Thus, a firm correlation can be established between the Tengchong volcano and the subduction and dehydration of the Indian continental slab or the Burma microplate (Lei et al., 2009b).

Because of its low density, the continental lithosphere has been traditionally assumed to be too light to be subducted. However, several processes contribute to the subduction of the continental lithosphere (Molnar and Gray, 1979). One is the negative buoyancy of the relative cold mantle part of continental lithosphere, which is consistent with previous studies (Forsyth and Uyeda, 1975; Turcotte and Schubert, 1982; Shemenda, 1993; Cloos, 1993). Another mechanism is the pull of a downgoing slab of oceanic lithosphere on continental lithosphere trailing behind it. Recent studies have demonstrated the process of continental crust subduction even down to the mantle transition zone, based on geological, geophysical and numerical modeling studies (e.g., Senshu et al., 2009; Kawai et al., 2013, and references therein). In subduction zones, continental crust is generated through arc magmatism and part of it is returned to the mantle through sediment subduction, subduction erosion, and continental subduction. Kawai et al. (2013) based on first principles calculations showed that continental crust can be subducted down to 660 km depth. The best natural example for deep subduction of continental crust comes from ultrahigh-pressure metamorphic rocks, some of which record diamond-facies conditions (e.g., Dobrzhinetskaya, 2012). In the Burma region, the negative buoyancy could be the primary force that causes the subduction of the Indian continental slab, due to the absence of oceanic slab. The lower crust above the subducting continental slab could transform to eclogite around 100 km depth, which would contribute to the negative buoyancy proportionally to the volume of the continental crust (Ranalli et al., 2000), because eclogite is denser than the surrounding mantle material down to the top of the mantle transition zone. The dehydration of the subducting slab might continue to depth because of the large amount of wet sediments being dragged down (Regenauer-Lieb et al., 2001).

Such a model may explain how and why the 10 March 2011 Yingjiang, China, earthquake (M 5.8) and the 24 March Burma (M 7.2) earthquake (Fig. 5) occurred (Lei et al., 2012a). The 4 February 2011 Indo-Burma earthquake occurred at ~90 km depth, suggesting that the Indian plate is still active and currently subducting eastward. The Yingjiang earthquake could be closely related to fluids contained in the upwelling flow under the Tengchong volcano. These fluids could enhance the stress concentration on the seismogenic layer, as well as decrease the effective normal stress across the fault planes of the Da Yingjiang fault. The occurrence of the 24 March Burma earthquake is quite similar (Lei et al., 2012a).

2.3. The Hainan volcano

The Hainan volcano is located at the Hainan island in the southernmost portion of the South China block and is separated from Mainland China by the Qiongzhou strait (Fig. 1). The Hainan volcano erupted several times since the Eocene. The Pliocene and Quaternary volcanism at the Hainan island can be grouped into two major eruptive stages, late Tertiary and Quaternary and mainly distributed in six eruptive areas, Chinniuling, Penglei-Geding, Lungtang, Yangpukang, Towenling, and Maanling (Ho et al., 2000). The volcanic eruption generated excellent physiographic features, but all the craters are not that high and the highest crater is only ~222.8 m above sea level (Fig. 2d,e). The basaltic lava flows are widely distributed and cover an area of over 7000 km^2 including the Leizhou peninsula, and the number of volcanic craters that can be distinguished amount to 177 (Liu, 2000). Such intensive Cenozoic magmatism should have connection with the deep structure of the region. Based on the low-V anomalies in the upper mantle and thinned mantle transition zone under the Hainan hotspot, a plume was hypothesized by Lebedev et al. (2000). Recent studies confirmed that the Hainan volcano to be of hotspot-type (e.g., Lebedev and Nolet, 2003; Liang et al., 2004; Montelli et al., 2004; Zhao, 2007).

Petrological results showed a high potential mantle temperature of 1400–1660°°C that is 100–360 °C higher than the normal temperature of basalt mantle (Yan and Shi, 2007; Wang, 2011; Hoang and Flower, 1998), suggesting the existence of thermal anomalies under the Hainan mantle. This supports the concept of the Hainan plume. However, from the ocean-bottom magnetic anomaly observations, it was inferred that the South China Sea spreading started from 32 Ma and culminated at 15.5 Ma (Briais et al., 1993; Kido et al., 2001). The volcanism in the South China Sea may be divided into three periods, pre-spreading (>32 Ma), syn-spreading (32–16 Ma) and post-spreading (<16 Ma), with distinct features in the spatial distribution of magmatic activity during different periods (Xu et al., 2012b). The distribution of Cenozoic volcanic rocks in South China Sea and surrounding regions seems to indicate the effect of the mid-oceanic ridge suction on the Hainan plume, but there are no features of volcanic rifted margins in the transition zone between the South China continental margin and South China Sea basin (Xu et al., 2012b). These discrepancies led to the debate on whether the Hainan plume has any impact on the South China Sea spreading (Xu et al., 2012b).

A large amount of geophysical data is available from the Hainan volcanic field. Seismic explosion experiments reveal a thinner crust with low-V anomalies under the Hainan volcanic field (e.g., Jia et al., 2006). Local seismic tomographic models inferred from arrival time data recorded at portable seismic stations demonstrate low-Vp and low-Vs anomalies around the northern Hainan island and these low-V anomalies extend northward above 20 km depth (Ding et al., 2004). Pn tomographic model shows a prominent low-V anomaly in the uppermost mantle (Liang et al., 2004). Global tomographic models illustrate pronounced low-V anomalies under the Hainan down to the lower mantle (Fig. 9), and suggest that the Hainan plume originated from the lower mantle (e.g., Zhao, 2004; Lei and Zhao, 2006a; Montelli et al., 2006). The U–Th disequilibrium data and Nd isotopic compositions support the mode of the lower mantle origin of the Hainan plume (e.g., Zou and Fan, 2010). However, some differences exist between these two tomographic models with regard to depth ranges. Lei and Zhao (2006a) and Zhao (2007) show a low-V anomaly extending down to the lowermost mantle (Fig. 9A), whereas Montelli et al. (2006)

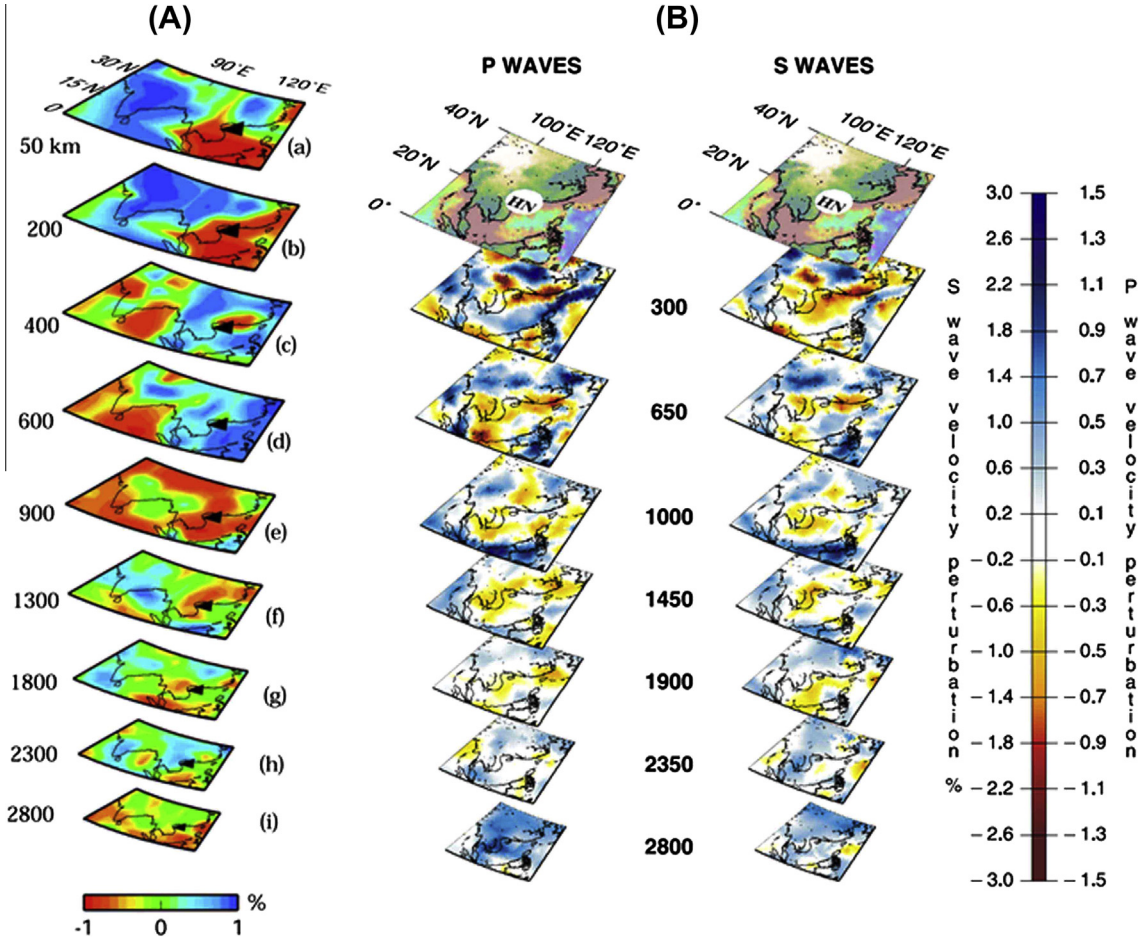

Fig. 9. Global velocity models in map view at different depths under the Hainan island. Red and blue colors denote low-V and high-V anomalies. The triangle denotes the Hainan hotspot. (A) The P-wave velocity model from Lei and Zhao (2006a); (B) The P-wave and S-wave velocity models from Montelli et al. (2006).

demonstrates a low-V anomaly down to only the middle mantle (Fig. 9B). These differences may be due to the different data sets used. Montelli et al. (2006) used only P, pP and PP seismic phases, whereas Lei and Zhao (2006a) and Zhao (2007) used ten types of seismic phases, such as P, pP, PP, PcP, Pdiff, PKPab, PKPbc, PKKPab, PKKPbc, PKiKP, which have a good coverage of seismic rays in the lowermost mantle around the Hainan island. However, the shallower structure of the Hainan plume is still unclear.

Lei et al. (2009a) picked 850 high-quality teleseismic P-wave arrival time data from original seismograms of 138 teleseismic events recorded at 9 seismic stations of the Hainan provincial network (Fig. 10a). Integrating with 3500 local arrival time data from selected 464 earthquakes, Lei et al. (2009a) obtained a clear image of the Hainan plume down to 300 km depth (Fig. 10b–d), which shows a southeastward titled low-V anomaly with depth under the Hainan island. Such a tilt of the plume is also supported by magnetotelluric results (Hu et al., 2007) and could be related to the double-sided subduction realms: the eastward subduction of the Indian slab and the westward subduction of the Philippine Sea slab (Qu et al., 2007; Liu et al., 2008a; Zhao and Liu, 2010), but the most likely explanation is that the plume was distorted by the lower mantle flow and then rose directly upward to the upper mantle (Steinberger and Antretter, 2006). This is supported by the existence of the ultra-low-V anomalies in the lowermost mantle around the Philippine island as seen from waveform modeling (Idehara et al., 2007).

2.4. The Datong volcano

The Quaternary Datong volcano is located in the northernmost portion of the Shanxi rift (Fig. 1). There are 30 small volcanoes in the Datong volcanic filed, and they are distributed about 3 km away from the Datong county. The volcanic field can be mainly divided into two domains: a northern area where at least 13 volcanic cones are distributed and a southeastern area where the volcanic cones have a small height (Xu et al., 2005). Potassium–Argon (K–Ar) dating constrains the timing of volcanism in the northern area as late Pleistocene (~0.4 Ma), which is later than that in the southeastern area since early Pleistocene (~0.74 Ma) (Chen et al., 1992). However, the mechanism of the origin of the Datong volcano has remained unclear.

Recent regional tomographic models showed low-V anomalies under the Datong volcano in the upper mantle (e.g., Tian et al., 2009; Zhao et al., 2009b). However, we cannot judge whether these low-V anomalies are related to the dehydration of the stagnant Pacific slab in the mantle transition zone under eastern China because the Datong volcano is about 2400 km away from the Japan Trench (Fig. 1). To examine the correlation between the Pacific subduction and the Datong volcanism, some researchers inverted the tomographic images on a large scale, and their models illustrate obvious low-V anomalies in the upper mantle under the volcano that are connected westward to those under the Japan Islands (e.g., Huang and Zhao, 2006; Li and van der Hilst, 2010). The results

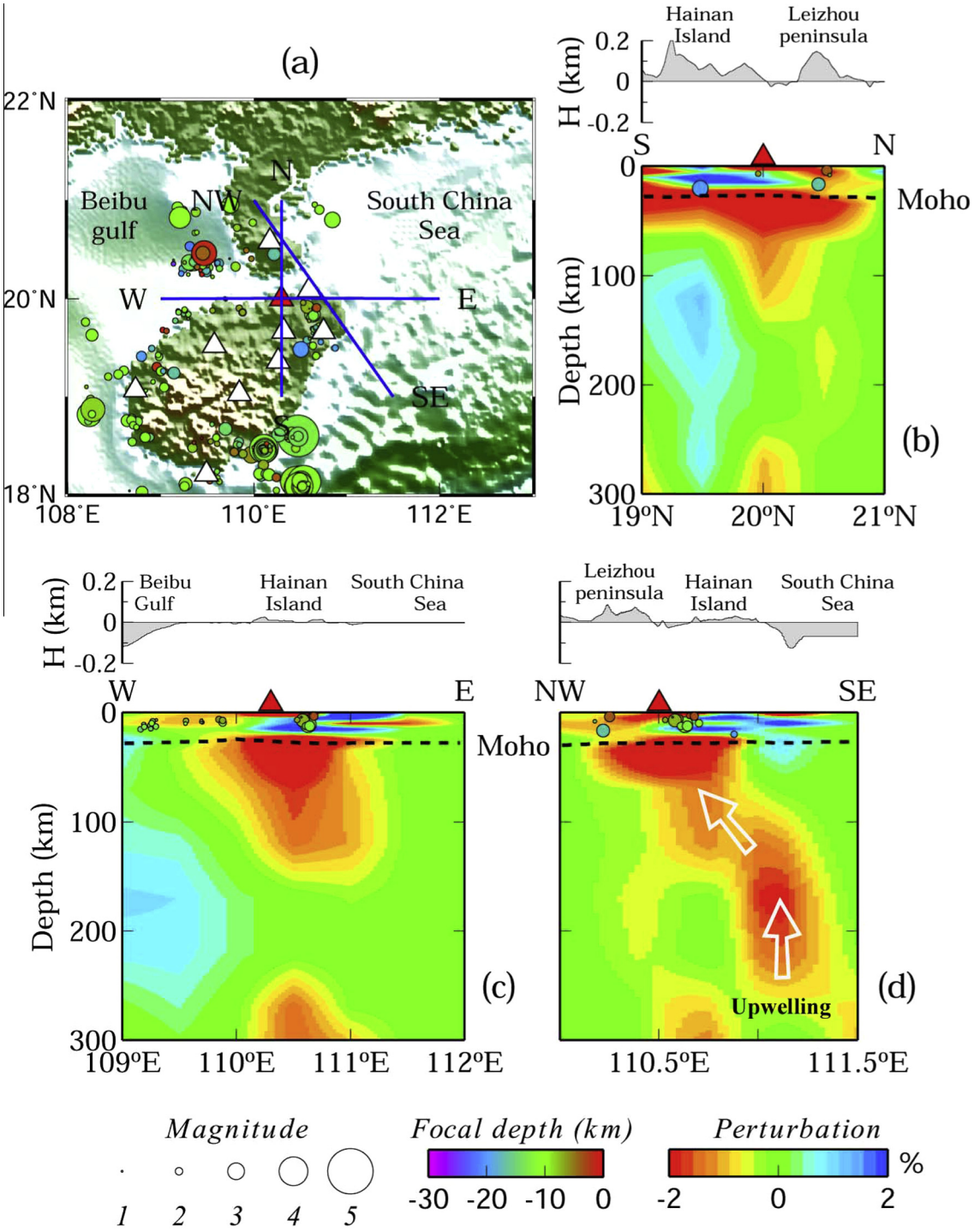

Fig. 10. (a) Locations of the Hainan hotspot (red triangle), vertical cross-sections (blue lines), seismic stations (open triangles), and local earthquakes (circles) used by Lei et al. (2009a). The scales for earthquake magnitude and focal depth are shown at the bottom of (c,d). (b–d) P-wave tomographic images (Lei et al., 2009a) along these three vertical cross sections. Red and blue colors denote low-V and high-V anomalies. The scale for velocity perturbation is shown at the bottom. Dashed lines denote the Moho discontinuity, while color circles denote the earthquakes within 25 km off the profiles. The topography along the cross-sections is shown on the top.

seemly suggest that the deep origin of Datong volcano could be related to the subduction of the Pacific slab. To demonstrate such a correlation, Lei (2012) collected a large number of high-quality arrival-time data recorded at provincial seismic networks in the North China Craton and manually picked from original seismograms (Zheng et al., 2009, 2010) of teleseismic events. His tomographic model shows an obviously Y-shaped low-V anomaly under the Datong volcano and Bohai Sea, and this low-V anomaly extends down to the lower mantle (Figs. 11 and 12), suggesting that the Datong volcano might originate from the lower mantle. It is also found that the high-V anomalies representing the stagnant Pacific slab in the mantle transition zone show a clear gap (Fig. 11g and h), which may correspond to the upwelling of the hot material from the lower mantle. A vertical view of tomographic image illustrates the low-V anomalies under the Datong volcano ascending from the lower mantle to about 200 km depth and then branching out (Fig. 12). One of these branches ascends eastward to under the Bohai Sea, whereas the other moves westward to under

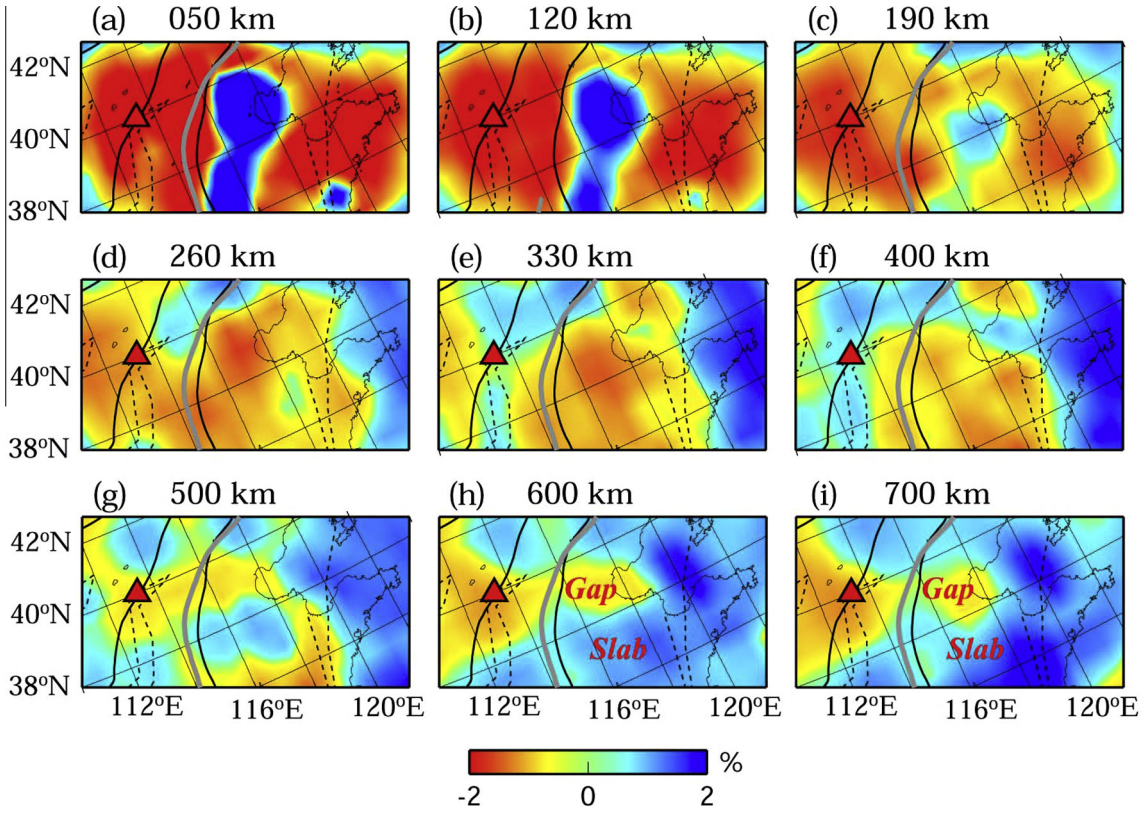

Fig. 11. Tomographic images (Lei, 2012) under the Datong volcano (red triangle) in map view. Red and blue colors denote low-V and high-V anomalies, respectively. The color scale for velocity perturbation is shown at the bottom. Solid and black lines denote the boundaries of the eastern, western and central North China Cratons. The gray line marks the North–South Gravity lineament. Dashed lines denote the Shanxi rift and Tanlu fault zone, respectively.

the Datong volcano (Fig. 12). From these results Lei (2012) concluded that the origin of the Datong volcano is more likely from the lower mantle, although it may be related to the dehydration and deep subduction of the Pacific slab that is stagnant in the mantle transition zone. This is somewhat similar to that of the Yellowstone plume, where low-V anomalies may penetrate the gap of the Farallon slab from the lower mantle to the upper mantle (Xue and Allen, 2007; Liu and Stegman, 2012; Tian and Zhao, 2012). Such a gap of the stagnant Pacific slab in the mantle transition zone could be caused by slab tearing due to differential movement (Obayashi et al., 2009). A similar tearing is also reported under the Italian peninsula (Rosenbaum et al., 2008). Another possibility is the instability of the stagnant Pacific slab in the mantle transition zone due to the gravity influence related to the phase changes (Ai et al., 2008). The lower mantle origin of the Datong volcano could be related to either the collapsed slab in the mantle transition zone down to the lower mantle ascribed to the gravity influence (Zhu et al., 2011) or to the existence of the thermal boundary layer at certain depth in the lower mantle (Sleep et al., 1988; Steinberger and Torsvik, 2012). Therefore, the model of Lei (2012) does not only explain the mechanism of the formation of the Datong volcano, but also supports the concept of the Bohai plume hypothesized by Teng et al. (1997). Under the Bohai Sea area there are a higher thermal gradient, a shallower Moho discontinuity, diffused stress field and shallower high-conductive layers in the upper mantle, the channels for hot material upwelling in the crust, and buried basalts beneath the surface (Teng et al., 1997).

2.5. The Xing'an-Mongolia volcanic group

The Xing'an-Mongolia volcanic group mainly includes the Nuomin-river volcanoes, the Halaha-river volcanoes, and the Abaga volcanoes from northeast to southwest along the North–South Gravity Lineament (Fig. 1). They could be active, because their last eruptions were in the Holocene time (Fig. 2f,g) (e.g., Bai et al., 2005, 2008; Zhao et al., 2008; Fan et al., 2011, 2012). Global and large-scale regional tomographic models are too generalized to see significant deep structures related to these volcanoes on the surface (e.g., Zhao, 2004; Lei and Zhao, 2006a; Huang and Zhao, 2006), whereas detailed seismic tomography has been seldom conducted, because few seismic stations are installed and few events occurred there. However, recent geochemical and petrological studies have contributed to a better understanding of magmatism associated with these active volcanoes. From investigations of volcanic field and K–Ar dating, the activities of both the Halaha-river volcanoes and Nuomin-river volcanoes can by divided into four periods, the early Pleistocene, middle Pleistocene, late Pleistocene, and Holocene (Fan et al., 2011, 2012). However, distinct differences can be noticed between these two volcanic groups in major active periods. For the Halaha-river volcanoes, the most active period was in the middle Pleistocene, and the volcanism became weak in the late Pleistocene but strong again in the Holocene (Fan et al., 2011). For the Nuomin-river volcanoes, the middle Pleistocene marks the flare-up with the most intensive activity during the Quaternary, and the volcanism became weak in the late Pleistocene and Holocene (Fan et al., 2012).

The Abaga volcanic field is situated in the southern end of the Xing'an-Mongolia orogenic belt. Analyses of the mantle peridotite xenoliths from this Abaga volcanic field show a medium–low-temperature thermal state and a fertile-transitional lithospheric mantle, which is similar to the Datong volcanic field but different from the Halaha-river volcanic field that displays an ancient lithospheric mantle (Chen et al., 2012b). These differences suggest that the Xing'an-Mongolia orogenic belt has prominently temporal-

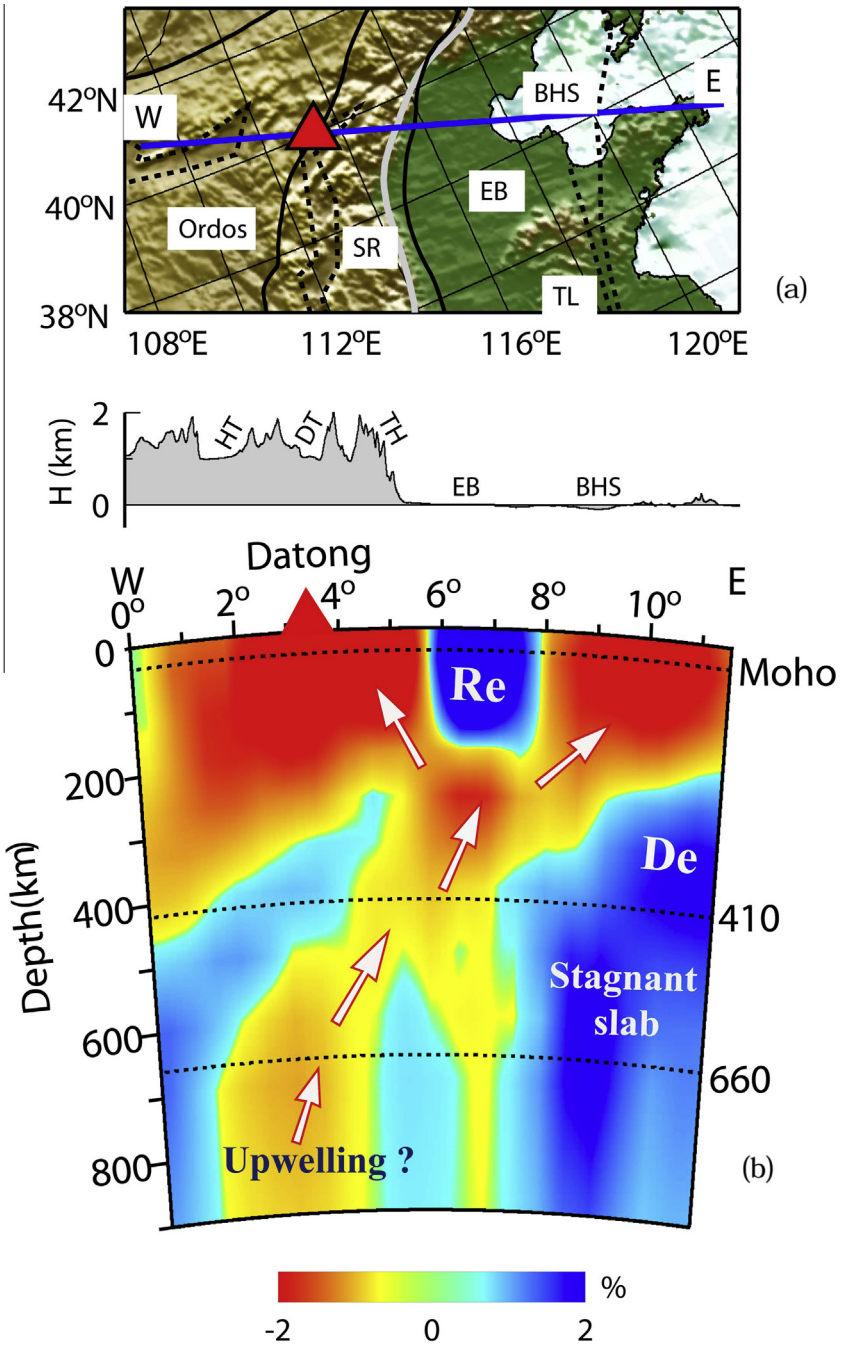

Fig. 12. Tomographic images (Lei, 2012) under the Datong volcano (DT, red triangle) along the vertical cross-section from northwest to southeast. HT, the Hetao rift; TH, the Taihang mountain; EB, eastern block of North China Craton; SR, the Shanxi rift; TL, the Tanlu fault zone; BHS, the Bohai Sea. Re, residual of detached lithosphere; De, detached lithosphere. Other symbols are the same as shown in Fig. 11.

spatial heterogeneities in the lithospheric mantle. The primary causes of these contrasts were summarized by Chen et al. (2012b). First, the Xing'an-Mongolia orogenic belt consists of different blocks, the Halaha-river volcanic field is in the Xing'an block that has been stable since the early Paleozoic, while the Abaga volcanic field is on the Songnei block that was unstable until the late Paleozoic. (2) The Abaga volcanism was much stronger than that in the Halaha-river volcanic areas, possibly indicating that the ancient lithospheric mantle has partially been eroded and transformed to the young lithospheric mantle in the Abaga area (Zhang et al., 2007; Tang et al., 2008). (3) The carbonic fluid inclusions occurring in the peridotite xenoliths in the Abaga volcanic area (Kononova et al., 2002) suggest transformation of harzburgite into lherzolite (Ionov et al., 1996), which made the Abaga region different from other regions in the Xing'an-Mongolia region.

3. Discussion

3.1. Seismic tomography with integrated data

To obtain the deep structure down to the mantle transition zone, teleseismic arrival time data are usually used in the tomographic technique (Zhao et al., 1994; Hung et al., 2004; Rawlinson et al., 2006). However, teleseismic rays are nearly vertical in the

shallow crust, and therefore teleseismic tomography cannot resolve the crustal structure well. To yield a good criss-cross ray coverage in the shallow crust to better image the mantle structure, local and teleseismic data were integrated during tomographic inversion under the Tengchong and Hainan volcanoes (Figs. 3B, 6, 7 and 10) (e.g., Lei et al., 2009a, 2009b), whereas the mantle structures under the Changbaishan and Datong volcanoes were imaged by correcting the theoretical teleseismic travel times (Figs. 3A, 11, 12) (e.g., Lei and Zhao, 2005; Koulakov et al., 2009; Lei, 2012) with an existing 3-D velocity crustal model containing an undulating Moho discontinuity, such as the CRUST2.0 model (Mooney et al., 1998; Bassin et al., 2000). These two kinds of tomographic techniques can avoid mapping crustal structure into the mantle and *vice versa* and they have been popularly adopted to invert the mantle structure in various regions of the world, such as under the Japan Islands, Iceland, Tienshan orogenic belt, and Anatolian plateau (e.g., Zhao et al., 1994, 1996, 2012a; Hung et al., 2004; Lei and Zhao, 2007a,b). Recently, some researchers applied a joint inversion of complementary body and surface wave data that can close the gap between well resolved lithospheric and mantle structures on global scale and under Iceland, US and China (e.g., Allen et al., 2002; Antolik et al., 2003; West et al., 2004; Obrebski et al., 2011, 2012). A future attempt should focus on a joint inversion of body and surface wave data under the volcanoes in China.

3.2. Seismic tomography with later phases

Tomographic images (Figs. 3, 6, 7 and 10–12) shown in the present study were obtained using only the direct P-wave arrival times, because the direct waves usually have a relative higher accuracy than later phases. However, later phases often sample the Earth's mantle structure not ordinarily sampled by the direct P waves in most portions of the crust and mantle. Therefore, adding later phases is considered to be an effective way to improve the tomographic image, particularly for the regions where few seismic stations and events exist. In global tomographic studies a number of later seismic phases have been used to enhance the ray coverage in the southern hemisphere and oceanic regions (e.g., Vasco and Johnson, 1998; Boschi and Dziewonski, 2000; Karason and van der Hilst, 2001; Zhao, 2001, 2004, 2007; Lei and Zhao, 2006a). Zhao (2001, 2004, 2007) used arrival times of P, pP, PP, PcP and Pdiff phases to invert for global tomographic images to decipher the deep structure of the mantle plumes. In addition to these later seismic phases, Lei and Zhao (2006a, 2006b) added more later phases that penetrate through the outer core, such as PKPab, PKPbc, PKiKP, PKKPab, PKKPbc, to obtain a new tomographic image. Their results have imaged the Hawaiian plume as a continuous low-V anomaly from the surface to the core-mantle boundary (Lei and Zhao, 2006a, 2006b), which significantly improved previous tomographic images of Obayashi and Fukao (1997), Zhao (2001, 2004), Fukao et al. (2003) and Montelli et al. (2004) and strongly suggested that the Hawaiian plume indeed originates from the lowermost mantle.

To demonstrate the effect of later seismic phases on the local tomographic inversion, Zhao et al. (2005) used S, SmS and sSmS arrival time data recorded at two seismic stations (GSC and PFO) that are 200 km apart and inverted crustal seismic structures around the Landers source areas. They found that later seismic phases significantly improve the crisscrossing ray coverage in the mid-lower crust. The inverted results illustrated that adding reflected seismic phases is a very effective way to improve the quality of tomographic images (Zhao et al., 2005). Although it is hard to accurately pick up the arrival times of later phases, this technique has been used in several different regions (e.g., Salah et al., 2005; Xia et al., 2007; Sun et al., 2008; Lei et al., 2008, 2011). Lei and Zhao (2006a, 2006b) investigated the effects of various mantle and core phases on the global mantle structure, and found that PP rays can provide a better constraints on the structure down to the middle mantle, in particular for the upper mantle under the oceans. PcP can enhance the ray sampling of the middle and lower mantle around the Pacific rim and Europe, while Pdiff can help improve the spatial resolution in most parts of the lowermost mantle. The outer core phases, PKP, PKiKP and PKKP, can improve the resolution in the lowermost mantle under the southern hemisphere and oceanic region.

In the teleseismic tomographic studies, recent researchers tried to use some later phases, such as pP, sP, ScP, PcP, PKiKP and PP phases, in their teleseismic tomographic inversion (Rawlinson and Kennett, 2008; Rawlinson et al., 2010), and found that later phases play important roles in imaging the upper mantle structure. Therefore, it is suggested to add later phases in imaging the deep structure under the Chinese volcanoes in the future.

3.3. Ray-theory tomography versus finite-frequency tomography

Tomographic images (Figs. 3, 6, 7, 9A, and 10–12) shown in the present study were inferred using the ray-theory travel-time tomographic technique of Zhao et al. (1994). In conventional travel time tomography, the linearized ray theory is commonly utilized to interpret a travel time shift relative to a value predicted for a radially symmetric Earth model. Propagation of a seismic wave within the heterogeneous Earth is regarded as a ray traveling along its infinitely thin geometrical path. However, in reality, wave front healing, scattering, and other diffraction phenomenon around velocity heterogeneities render the travel time of an actual finite-frequency wave sensitive to 3-D wave speed perturbation off the ray path (e.g., Dahlen et al., 2000; Hung et al., 2004). The Born-Frechet kernels for seismic travel time can explicitly express the influence of velocity heterogeneity off the ray path upon a finite-frequency travel-time shift. A simple model comparison between results from ray-theory and finite-frequency tomographic techniques suggests that the effect of the Born-Frechet kernels on the pattern and amplitude of velocity anomalies appears to be markedly smaller than that of damping and smoothing regularizations and errors in the data, thus the advantage of finite-frequency tomography over tomographic images could be overstated (van der Hilst and de Hoop, 2005). Dahlen and Nolet (2005) commented that their critique of the theoretical methodology is based upon the incorrect notion that one can account for errors in the synthetic pulse and/or origin time of an earthquake by a modification of the Frechet kernels expressing the first-order dependence upon the velocity perturbations. Nevertheless, the finite-frequency tomography can yield a reasonable amplitude of velocity anomalies on local, regional and global scales (e.g., Hung et al., 2004; Montelli et al., 2004; Tong et al., 2011, 2012), and it is still being used in the investigation of mantle structure under North America (e.g., Sigloch et al., 2008; Obrebski et al., 2010), Europe (e.g., Ren et al., 2012), Tibetan plateau (e.g., Ren and Shen, 2008; Hung et al., 2010), North China (e.g., Zhao et al., 2009b), and some specific areas like hotspots (Hung et al., 2004; Yang et al., 2006). In order to obtain more accurate amplitude of resolved velocity anomalies of the crust and upper mantle to better understand the magmatic activities under the volcanoes, it is suggested to conduct finite-frequency tomography around the Chinese volcanoes.

3.4. Anisotropic tomography

Tomographic images (Figs. 3, 6, 7, 9, 10 and 12) were deduced by assuming that the Earth is isotropic, but anisotropy actually exists in the real Earth's interior. Since early 1990s, shear wave splitting analysis has been extensively applied to seismological data for detecting anisotropy in the Earth, leading to seismic anisotropy being observed at different depths from the crust down to the

core-mantle boundary (Silver, 1996; Savage, 1999). The systematic analysis method was applied to local seismic waveform data, revealing the existence of obvious anisotropy in the middle and upper crust (e.g., Gao et al., 1998, 2011; Wu et al., 2009). Using Pms (Moho converted) seismic phase, the anisotropy in the entire crust was inferred (e.g., Sun et al., 2011; Chen et al., 2012a; Cheng et al., 2012). Using SKS splitting analyses, the anisotropic results within the lithosphere and/or asthenosphere can be derived (e.g., Wang et al., 2008; Zhao et al., 2007b, 2012b; Huang et al., 2011). In addition, there is growing observational evidence for significant anisotropy in the lowermost mantle (e.g., Lay et al., 1998; Wang and Wen, 2007; Long, 2009; He and Long, 2011). These results suggest extensive anisotropy in the medium of the Earth's interior at different depths (Crampin, 1981).

The existence of anisotropy in the Earth could affect the geometry and amplitude of resolved velocity anomalies, and thus Hearn (1996) took into account anisotropy in the uppermost-mantle tomography using Pn arrival time data. However, his model was parameterized into 2-D grid nodes in the horizontal directions. Recently, to obtain a 3-D anisotropic tomographic model, Ishise and Oda (2005) and Wang and Zhao (2008) developed a technique to relate travel time residuals to both lateral heterogeneities and anisotropy in the region of interest. Furthermore, the pattern of velocity anomalies is much clearer when the anisotropy is taken into account in the tomographic inversion. In mainland China, Huang et al. (2011) applied the shear-wave splitting techniques to core phases (SKS, SKKS, SKiKS and PKS) and direct S waves from regional and distant earthquakes recorded at 138 permanent seismic stations in mainland China, and found the existence of anisotropy at the stations around the Changbaishan and Tengchong volcanic fields, but it is much weaker than that in the surround areas. These results may indicate that only some, rather than all, parts of seismic rays used in the anisotropic analyses pass through the conduits of the hot material upwelling in the upper mantle under the region. A similar spatial distribution of the azimuthal anisotropy has been demonstrated using the data of Rayleigh waves (Yi et al., 2010). Thus, future work should also focus on anisotropic tomographic inversion in the volcanic region to better understand the deep structure and dynamics of the volcanoes in China.

3.5. Future work

Our present synthesis focused on seismic structures of the upper mantle around the Changbaishan, Tengchong, Hainan, and Datong volcanoes in evaluating their deep origins. However, the deep structures of the upper mantle around the Wudalianchi and Ashikule (Kunlun) volcanoes and Xing'an-Mongolia volcanic group have not been studied yet, mainly because of sparse seismic stations there. Since the initiation of the North China Craton destruction project by the National Natural Science Foundation of China, some broadband portable seismic networks have been deployed in northeast China. For example, a densely spaced portable seismic array was installed around the Wudalianchi volcano during June 2009 and June 2011 by the Institute of Geophysics, China Earthquake Administration, but these stations were aligned in two parallel NW oriented lines that are about 150–200 apart, and only the north line passes through the volcano (e.g., Zhang et al., 2013). The linear array is generally thought to be hard to give a good criss-cross coverage of seismic rays in the mantle. One more example is the NECESSArray seismic network that was deployed in northeastern China by the Sino-US-Japan cooperation from September 2009 to August 2011 (e.g., Guo et al., 2011). This network is a block-shaped array and can give a criss-cross ray coverage in the mantle, but the Wudalianchi volcano is immediately outside this network. Therefore, so far we have had no local tomographic images under the Wudalianchi volcano. In the Ashikule (Kunlun) volcanic field the Chinese provincial seismic stations are very sparse and there are no portable seismic arrays. Future attempts should therefore add more seismic stations around the Wudalianchin and Ashikule (Kunlun) volcanoes and Xing'an-Mongolia volcanic group and apply recently developed techniques as mentioned in Section 3 to obtain more reasonable seismic images to better understand the origins of the Chinese volcanoes.

4. Summary

A synthesis of the recent results on the deep structures under the volcanoes in China leads to the following conclusions. The Changbaishan volcano is a back-arc volcano which is closely related to the dynamic processes of the hot material upwelling in the big mantle wedge (BMW) due to the stagnancy and dehydration of the Pacific slab in the mantle transition zone. The Tengchong volcano is somewhat similar to that of the Changbaishan volcano and is associated with the subduction of the Indian plate or Burma microplate, and its main distinction from the Changbaishan volcano is the continental subduction. The Hainan volcano could be a hotspot-type, which is different from the Changbaishan and Tengchong intraplate volcanoes. The Hainan plume may have its origin in the lower mantle, and the tilt of the Hainan plume could be related to the lower mantle flow. Similar to the Hainan volcano, the Datong volcano could also be a lower mantle plume, though it is somewhat related to the dehydration of the stagnant Pacific slab in the mantle transition zone. These results would be of great significance to understand the dynamics of East Asia and to mitigate the volcanic hazards in the future. Future work should improve the density and morphology of seismic arrays around the volcanoes and utilize the recently developed seismic tomographic techniques to obtain more reasonable images under these volcanoes.

Acknowledgements

We thank Prof. Dapeng Zhao for thoughtful discussion. This work was partially supported by the National Natural Science Foundation of China (Nos. 41274059, 40974021 and 40774044) and Beijing Natural Scientific Foundation (Nos. 8122039 and 8092028) to J. Lei. This work also contributes to the 1000 Talents Award to M. Santosh from the Chinese Government. The GMT software package distributed by Wessel and Smith (1995) was used for plotting most figures. We thank Prof. G. Helffrich and two anonymous reviewers for providing many constructive comments and suggestions, which improved manuscript.

References

Abdelwahed, M., Zhao, D., 2007. Deep structure of the Japan subduction zone. Physics of the Earth and Planetary Interiors 162, 32–52.
Ai, Y., Zheng, T., Xu, W., He, Y., Dong, D., 2003. A complex 660 km discontinuity beneath northeast China. Earth and Planetary Science Letters 212, 63–71.
Ai, Y., Zheng, T., Xu, W., Li, Q., 2008. Small scale hot upwelling near the North Yellow Sea of eastern China. Geophysical Research Letters 35, L20305.
Allen, R., Nolet, G., Morgan, W., et al., 2002. Imaging the mantle beneath Iceland using integrated seismological techniques. Journal of Geophysical Research 107 (B12), 2325.
Antolik, M., Gu, Y., Ekstrom, G., Dziewonski, A.M., 2003. J362D28: a new joint model of compressional and shear velocity in the Earth's mantle. Geophysical Journal International 153, 443–466.
Bai, Z., Tian, M., Wu, F., Xu, D., Li, T., 2005. Yanshan and Gaoshan: two active volcanoes of the volcanic cluster of Arshan, Inner Mongolian. Earthquake Research in China 21, 113–117.
Bai, Z., Wang, J., Xu, G., Liu, L., Xu, D., 2008. Quaternary volcano cluster of Wulanhada, Right-back-banner, Chahaer, Inner Mongolia. Acta Petrologica Sinica 24 (11), 2585–2594.
Bassin, C., Laske, G., Masters, G., 2000. The current limits of resolution for surface wave tomography in North America. EOS Transition of AGU 81, F897.

Basu, A., Wang, J., Huang, W., 1991. Major element, REE, and Pb, Nd and Sr isotropic geochemistry of Cenozoic volcanic rocks of eastern China: implications for their origin from suboceanic-type mantle reservoirs. Earth and Planetary Science Letters 105, 149–169.
Bijwaard, H., Spakman, W., Engdahl, E.R., 1998. Closing the gap between regional and global travel time tomography. Journal of Geophysical Research 103, 30055–30078.
Boschi, L., Dziewonski, A., 2000. Whole Earth tomography from delay times of P, PcP and PKP phases: lateral heterogeneities in the outer core or radial anisotropy in the mantle? Journal of Geophysical Research 105, 13675–13696.
Briais, A., Patriat, P., Tapponnier, P., 1993. Updated interpretation of magnetic anomalies and seafloor spreading stages in the South China Sea: implications for the Tertiary tectonics of Southeast Asia. Journal of Geophysical Research 98, 6299–6328.
Chen, W., Li, D., Dai, T., 1992. The K–Ar age and excess Ar of quaternary basalt in Datong. In: Liu, R. (Ed.), The Age and Geochemistry of Cenozoic Volcanic Rock in China. Seismology Press, Beijing, pp. 81–92.
Chen, Y., Zhang, Z., Sun, C., Badal, J., 2012a. Crustal anisotropy from Moho converted Ps wave splitting analysis and geodynamic implications beneath the eastern margin of Tibet and surrounding regions. Gondwana Research. Available at: <http://dx.doi.org/10.106/j.gr.2012.04.003>.
Chen, S., Fan, Q., Zhao, Y., Sui, J., Du, X., 2012b. Mantle peridotite xenoliths and the nature of lithospheric mantle in Abagam Inner Mongolia. Acta Petrologic Sinica 28 (4), 1108–1118.
Cheng, C., Chen, L., Yao, H., Jiang, M., Wang, B., 2012. Distinct variations of crustal shear wave velocity structure and radial anisotropy beneath the North China Craton and tectonic implications. Gondwana Reseach. Available at: <http://dx.doi.org/10.106/j.gr.2012.02.014>.
Cloos, M., 1993. Lithospheric buoyancy and collisional orogenesis, subduction of oceanic plateaus, continental margins, island arcs, spreading ridges, and seamounts. Geological Society of America Bulletin 105, 715–737.
Conder, J., Wiens, D., 2006. Seismic structure beneath the Tonga arc and Lau back-arc basin determined from joint Vp, Vp/Vs tomography. Geochemistry Geophysics Geosystems 7, Q03018.
Crampin, S., 1981. A review of wave motion in anisotropic and cracked elastic-media. Wave Motion 3, 343–391.
Dahlen, F., Nolet, G., 2005. Comment on On sensitvity kernels for wave-equation transmission tomography by de Hoop and van der Hilst. Geophysical Journal International 163, 949–951.
Dahlen, F., Hung, S., Nolet, G., 2000. Frechet Kernels for finite-frequency traveltimes–Theory, I. Geophysical Journal International 141, 157–174.
Deng, Q., Zhang, P., Ran, Y., Yang, X., Mi, W., Chu, Q., 2002. General characteristics of China active tectonics. Science in China Series D: Earth Science 32 (12), 1021–1030.
Ding, Z., Li, W., Wu, Q., Hu, J., He, Z., Zhang, L., 2004. Seismological observations and velocity structure of the crust and upper mantle in the north Hainan volcanic region. In: Zhang, Z., Gao, R., Lv, Q., Liu, Z. (Eds.), Earth's deep structure and dynamics of mainland China—the 50-th Anniversary of Academician Teng working for geophysics, Scientific Press, Beijing, pp. 846–857.
Dobrzhinetskaya, L.F., 2012. Microdiamonds-Frontier of ultrahigh-pressure metamorphism: a review. Gondwana Research 21, 207–223.
Duan, Y., Zhao, D., Zhang, X., Xia, S., Liu, Z., Wang, F., Li, L., 2009. Seismic structure and origin of active intraplate volcanoes in Northeast Asia. Tectonophysics 470, 257–266.
Ekstrom, G., Dziewonski, A., Maternovskaya, N., Nettles, M., 2005. Global seismicity of 2003: centroid-moment-tensor solutions for 1087 earthquakes. Physics of the Earth and Planetary Interiors 148, 327–351.
Engdahl, R., van der Hilst, R., Buland, R., 1998. Global teleseismic earthquake relocation with improved travel times and procedures for depth determination. Bulletin of the Seismological Society of America 88, 722–743.
England, P., Houseman, G., 1986. Finite strain calculations of continental deformation: 2. Comparison with the India-Asia collision zone. Journal of Geophysical Research 91, 3664–3676.
Fan, Q., 2005. Watching on the volcano. China. Chinese Journal of Nature 1, 42–51.
Fan, Q., Hooper, P., 1991. The Cenozoic basaltic rocks of eastern China: petrology and chemical composition. Journal of Petrology 32, 765–810.
Fan, Q., Liu, R., Li, D., Li, Q., 1998. Significance of K–Ar age of bimodal volcanic rocks at Wangtiane's Volcano, Changbaishan area. Chinese Science Bulletin 43, 2222–2225.
Fan, Q., Liu, R., Wei, H., Sui, J., Li, N., 1999. Holocene eruption and petrogeochemical characteristics of the Tianchi Volcano, Changbaishan Mountains. Geological Review 45 (Suppl.), 263–271.
Fan, Q., Sun, J., Liu, R., 2001. Sr–Nd isotopic geochemistry and magmatic evolutions of Wudalianchi volcano, Tianchi volcano and Tengchong volcano. Acta Petrologica et Mineralogica 20 (3), 233–238.
Fan, Q., Zhao, Y., Li, D., Wu, Y., Sui, J., Zheng, D., 2011. Studies on quaternary volcanism stages of Halaha river and Chaoer river area in the great Xing'an range: evidence from K–Ar dating and volcanic geological features. Acta Petrologica Sinica 27 (10), 2827–2832.
Fan, Q., Zhao, Y., Sui, J., Li, D., Wu, Y., 2012. Studies on quaternary volcanism stages of Nuomin river area in the great Xing'an range: evidence from petrology, K–Ar dating and volcanic geology features. Acta Petrologica Sinica 28 (4), 1092–1098.
Forsyth, D., Uyeda, S., 1975. On the relative importance of the driving force of plate motion. Geophysical Journal of Royal Astronomical Society 43, 163–200.
Fukao, Y., Obayashi, M., Inoue, H., 1992. Subducting slabs stagnant in the mantle transition zone. Journal of Geophysical Research 97, 4809–4822.
Fukao, Y., To, A., Obayashi, M., 2003. Whole mantle wave tomography using P and PP-P data. Journal of Geophysical Research 108. http://dx.doi.org/10.1029/2001JB000989.
Gao, Y., Wang, P., Zheng, S., et al., 1998. Temporal changes in shear-wave splitting at an isolated swarm of small earthquakes in 1992 near Dongfang, Hainan Island, southern China. Geophysical Journal International 135 (1), 102–112.
Gao, Y., Wu, J., Fukao, Y., Shi, Y., Zhu, A., 2011. Shear wave splitting in the crust in North China: stress, faults and tectonic implications. Geophysical Journal International 187, 642–654.
Gudmundsson, O., Sambridge, M., 1998. A regionalized upper mantle (RUM) seismic model. Journal of Geophysical Research 103, 7121–7136.
Guo, Z., Wilson, M., 2012. The Himalayan leucogranites: constraints on the nature of their crustal source region and geodynamic setting. Gondwana Research 22, 360–376.
Guo, Z., Hertogen, J., Liu, J., Pasteels, P., Boven, A., Punzalan, L., He, H., Luo, X., Zhang, W., 2005. Potassic magmatism in western Sichuan and Yunnan provinces, SE Tibet, China: petrological and geochemical constraints on petrogenesis. Journal of Petrology 46, 33–78.
Guo, Z., Liu, Z., Tang, Y., Chen, J., Ning, J., Grand, S., Niu, F., Kawakash, H., Tanaka, S., 2011. Crustal and mantle structures of northeast China from ambient noise tomography and receiver functions of the NECESSArray. Presented at 2011 Fall Meeting, AGU, San Francisco, California, 5–9 December.
He, X., Long, M., 2011. Lowermost mantle anisotropy beneath the northwestern Pacific: evidence from PcS, ScS, SKS, and SKKS phases. Geochemistry Geophysics Geosystems 12, Q12012.
Hearn, T., 1996. Anisotropic Pn tomography in the western United States. Journal of Geophysical Research 101, 8403–8414.
Hetland, E., Wu, F., Song, J., 2004. Crustal structure in the Changbaishan volcanic area, China, determined by modeling receiver functions. Tectonophysics 386, 157–175.
Ho, K., Chen, J., Juang, W., 2000. Geochronology and geochemistry of late Cenozoic basalts from the Leiqiong area, southern China. Journal of Asian Earth Sciences 18, 307–324.
Hoang, N., Flower, M., 1998. Petrogenesis of Cenozoic basalts from Vietnam: implication for origin of a diffuse igneous province. Journal of Petrology 39, 369–395.
Hu, J., Deng, B., Wang, W., Lin, Z., Xiang, X., Wang, L., 2007. Deep electronic anomaly in the M7.5 Qiongshan earthquake region and its relationship with future seismicity. Acta Seismologica Sinica 29 (3), 258–264.
Hu, J., Hu, Y., Xia, J., Chen, Y., Zhao, H., Yang, H., 2008. Crust-mantle velocity structure of S wave and dynamic process beneath Burma Arc and its adjacent regions. Chinese Journal of Geophysics 51 (1), 140–148.
Huang, J., Zhao, D., 2006. High-resolution mantle tomography of China and surrounding regions. Journal of Geophysical Research 111. http://dx.doi.org/10.1029/2005JB004066.
Huang, J., Zhao, D., Zheng, S., 2002. Lithospheric structure and its relationship to seismic and volcanic activity in southwest China. Journal of Geophysical Research 107. http://dx.doi.org/10.1029/2000JB000137.
Huang, X., Xu, Y., Karato, S., 2005. Water content in the transition zone from electrical conductivity of wadsleyite and ringwoodite. Nature 434, 746–749.
Huang, Z., Wang, L., Zhao, D., Mi, N., Xu, M., 2011. Seismic anisotropy and mantle dynamics beneath China. Earth and Planetary Science Letters 306, 105–117.
Hung, S., Shen, Y., Chiao, L., 2004. Imaging seismic velocity structure beneath the Iceland hot spot: a finite frequency approach. Journal of Geophysical Research 109, B08305.
Hung, S., Chen, W., Chiao, L., Tseng, T., 2010. First multi-scale, finite-frequency tomography illuminates 3-D anatomy of the Tibetan Plateau. Geophysical Research Letters 37, L06304.
Ichiki, M., Baba, K., Obayashi, M., Utada, H., 2006. Water content and geotherm in the upper mantle above the stagnant slab: interpretation of electrical conductivity and seismic P-wave velocity models. Physics of the Earth and Planetary Interiors 155, 1–15.
Idehara, K., Yamada, A., Zhao, D., 2007. Seismological constraints on the ultralow velocity zones in the lowermost mantle from core-reflected waves. Physics of the Earth and Planetary Interiors 165, 25–46.
Inoue, T., 1994. Effect of water on melting phase relations and melt composition in the system Mg_2SiO_4–$MgSiO_3$–H_2O up to 15 GPa. Physics of the Earth and Planetary Interiors 85, 237–263.
Ionov, D., O'Reilly, S., Genshaft, Y., et al., 1996. Carbonate-bearing mantle peridotite xenoliths from Spitsbergen: phase relationships, mineral compositions and trace-element residence. Contributions to Mineralogy and Petrology 125, 375–392.
Ishise, M., Oda, H., 2005. Three-dimensional structure of P-wave anisotropy beneath the Tohoku district, northeast Japan. Journal of Geophysical Research 110, B07304.
Iwamori, H., 2004. Phase relations of peridotites under H_2O-saturated conditions and ability of subducting plates for transportation of H_2O. Earth and Planetary Science Letters 227, 57–71.
Jia, S., Li, Z., Xu, C., Shen, F., Zhao, W., Yang, Z., Yang, J., Lei, Y., 2006. Crust structure features in Leiqiong depression. Chinese Journal of Geophysics 49 (5), 1385–1394.
Karason, H., van der Hilst, R., 2001. Tomograhic imaging of the lowermost mantle with differential times of refracted and diffracted core phases (PKP, Pdiff). Journal of Geophysical Research 106, 6569–6587.

Kato, N., Yoshida, S., 2011. A shallow strong patch model for the 2011 great Tohoku-oki earthquake: a numerical simulation. Geophysical Research Letters, 38, L00G04.
Kawai, K., Yamamoto, S., Tsuchiya, T., Maruyama, S., 2013. The second continent: existence of granitic continental materials around the bottom of the mantle transition zone. Geoscience Frontiers 4, 1–6.
Kido, Y., Suyehiro, K., Kinoshita, H., 2001. Rifting to spreading process along the northern continental margin of the South China Sea. Marinal Geophysical Research 22, 1–15.
Komabayashi, T., Omori, S., Maruyama, S., 2004. Petrogenetic grid in the system $MgO–SiO_2–H_2O$ up to 30 GPa, 1600 °C: applications to hydrous peridotite subducting into the Earth's deep interior. Journal of Geophysical Research 109, B03206.
Kononova, V., Kurat, G., Embey-Isztin, A., Perovov, V., Brandstatter, F., 2002. Geochemistry of metasomatised spinel peridotite xenoliths from the Dariganga plateau, south-eastern Mongolia. Mineralogy and Petrology 75, 1–21.
Koulakov, I., Kaban, M.K., Tesauro, M., Cloetingh, S., 2009. P- and S-velocity anomalies in the upper mantle beneath Europe from tomographic inversion of ISC data. Geophysical Journal International. http://dx.doi.org/10.1111/j.1365-246X.2009.04279.x.
Lay, T., Williams, Q., Garnero, E., Kellogg, L., Wyession, M., 1998. Seismic wave anisotropy in the D'' region and its implications. In: Gurnis, M., et al. (Eds.), The Core-Mantle Boundary Region, Geodyn. Ser., vol. 28, pp. 299–318.
Lebedev, S., Nolet, G., 2003. Upper mantle beneath Southeast Asia from S velocity tomography. Journal of Geophysical Research 108. http://dx.doi.org/10.1029/2000JB000073.
Lebedev, S., Chevrot, S., Nolet, G., van der Hilst, R., 2000. New seismic evidence for a deep mantle origin of the S. China basalts (the Hainan plume?) and other observations in SE Asia. EOS Transaction AGU 81, 48.
Lei, J., 2012. Upper-mantle tomography and dynamics beneath the North China Craton. Journal of Geophysical Research 117, B06313.
Lei, J., Zhao, D., 2005. P-wave tomography and origin of the Changbaishan intraplate volcano in Northeast Asia. Tectonophysics 397, 281–295.
Lei, J., Zhao, D., 2006a. Global P-wave tomography: on the effect of various mantle and core phases. Physics of the Earth and Planetary Interiors 154, 44–69.
Lei, J., Zhao, D., 2006b. A new insight into the Hawaiian plume. Earth and Planetary Science Letters 241, 438–453.
Lei, J., Zhao, D., 2007a. Teleseismic P-wave tomography and the upper mantle structure of the central Tien Shan orogenic belt. Physics of the Earth and Planetary Interiors 162, 165–185.
Lei, J., Zhao, D., 2007b. Teleseismic evidence for a subducting break-off slab under Eastern Turkey. Earth and Planetary Science Letters 257, 14–28.
Lei, J., Xie, F., Lan, C., Xing, C., Ma, S., 2008. Seismic images under the Beijing region inferred from P and PmP data. Physics of the Earth and Planetary Interiors 168, 134–146.
Lei, J., Zhao, D., Steinberger, B., Wu, B., Shen, F., Li, Z., 2009a. New seismic constraints on the upper mantle structure of the Hainan plume. Physics of the Earth and Planetary Interiors 173, 33–50.
Lei, J., Zhao, D., Su, Y., 2009b. Insight into the origin of the Tengchong intraplate volcano and seismotectonics in southwest China from local and teleseismic data. Journal of Geophysical Research 114, B05302.
Lei, J., Zhao, D., Xie, F., Liu, J., 2011. An attempt to detect temporal variations of crustal structure in the source area of the 2006 Wen-An earthquake in North China. Journal of Asian Earth Sciences 40, 958–976.
Lei, J., Xie, F., Mishra, O.P., Lu, Y., Zhang, G., Li, Y., 2012a. The 2011 Yingjiang, China, Earthquake: a volcano-related fluid-driven earthquake? Bulletin of the Seismological Society of America 102 (1), 417–425.
Lei, J., Zhang, G., Xie, F., Li, Y., Su, Y., Liu, L., Ma, H., Zhang, J., 2012b. Relocation of the 10 March 2011 Yingjiang, China, earthquake sequence and its tectonic implications. Earthquake Science 25, 103–110.
Li, C., van der Hilst, R., 2010. Structure of the upper mantle and mantle transition zone beneath Southeast Asia from traveltime tomography. Journal of Geophysical Research 115, B07308.
Li, X., Yuan, X., 2003. Receiver functions in northeast China—implications for slab penetration into the lower mantle in northwest Pacific subduction zone. Earth and Planetary Science Letters 216, 679–691.
Li, C., van der Hilst, R., Meltzer, A., Engdahl, E., 2008. Subduction of the Indian lithosphere beneath the Tibetan Plateau and Burma. Earth and Planetary Science Letters 274, 157–168.
Li, Y., Wu, Q., Pan, J., Sun, L., 2012. S-wave velocity structure of northeastern China from joint inversion of Rayleigh wave phase and group velocities. Geophysical Journal International 190, 105–115.
Liang, C., Song, X., Huang, J., 2004. Tomographic inversion of Pn travel times in China. Journal of Geophysical Research 109 (doi:10.1029/2003JB002789).
Liu, J., 1999. Chinese volcanoes. Science Press, Beijing, pp. 5–8.
Liu, R., 2000. Active volcanoes in China. Seismological Press, Beijing, pp. 11–44.
Liu, L., Stegman, D.R., 2012. Origin of Columbia River flood basalt controlled by propagating rupture of the Farallon slab. Nature 482, 386–390.
Liu, R., Wei, H., Li, J., et al., 1998. Recent eruption of the Changbaishan-Tianchi volcano. Science Press, Beijing, pp., 1–159.
Liu, M., Cui, X., Liu, F., 2004. Cenozoic rifting and volcanism in eastern China: a mantle dynamic link to the Indo-Asian collision? Tectonophysics 393, 29–42.
Liu, H., Hong, H., Ran, H., Shen, F., Zhao, B., Chen, H., 2008a. Dynamic mechanism of volcanic belt and new understanding from earthquake evidence in Northern Hainan island, China. Chinese Journal of Geophysics 51 (6), 1804–1809.
Liu, K., Gao, S., Gao, Y., Wu, J., 2008b. Shear wave splitting and mantle flow associated with the deflected Pacific slab beneath northeast Asia. Journal of Geophysical Research 113, B01305.
Long, M., 2009. Complex anisotropy in D'' beneath the eastern Pacific from SKS–SKKS splitting discrepancies. Earth and Planetary Science Letters 283, 181–189.
Maruyama, S., 1994. Plume tectonics. Journal of Geological Society of Japan 100, 24–49.
Molnar, P., Gray, D., 1979. Subduction of continental lithosphere: some constraints and uncertainties. Geology 7, 58–62.
Molnar, P., Tapponnier, P., 1975. Cenozoic tectonics of Asia: effects of a continental collision. Science 198, 419–426.
Montelli, R., Nolet, G., Masters, G., Dahlen, F., Hung, S., 2004. Global P and PP travel time tomography: rays versus waves. Geophysical Journal International 158, 637–654.
Montelli, R., Nolet, G., Dahlen, F., Masters, G., 2006. A catalogue of deep mantle plumes: new results from finite frequency tomography. Geochemistry Geophysics Geosystems 7. http://dx.doi.org/10.1029/2006GC001248.
Mooney, W., Laske, G., Masters, G., 1998. CRUST 5.1: a global crustal model at 55 degrees. Journal of Geophysical Research 103, 727–747.
Obayashi, M., Fukao, Y., 1997. P and PcP travel time tomography for the core-mantle boundary. Journal of Geophysical Research 102, 17825–17841.
Obayashi, M., Yoshimitsu, J., Fukao, Y., 2009. Tearing of stagnant slab. Science 324, 1173–1175.
Obrebski, M., Allen, R., Mei, X., Hung, S., 2010. Slab-plume interaction beneath the Pacific Northwest. Geophysical Research Letters 37, L14305.
Obrebski, M., Allen, R.M., Pollitz, F., Hung, S., 2011. Lithosphere-asthenosphere interaction beneath the western United States from the joint inversion of body-wave traveltimes and surface-wave phase velocities. Geophysical Journal International 185, 1003–1021.
Obrebski, M., Allen, R.M., Zhang, F., Pan, J., Wu, Q., Hung, S., 2012. Shear wave tomography of China using joint inversion of body and surface wave constraints. Journal of Geophysical Research 117, B01311.
Ohtani, E., Litasov, K., Hosoya, T., Kubo, T., Kondo, T., 2004. Water transport into the deep mantle and formation of a hydrous transition zone. Physics of the Earth and Planetary Interiors 143, 255–269.
Qu, C., Zhou, H., Zhao, D., 2007. Deep structure beneath the west margin of Philippine Sea Plate and South China Sea from P and S wave travel time tomography. Chinese Journal of Geophysics 50 (6), 1757–1768.
Ranalli, G., Pellegrini, R., D'Offizi, S., 2000. Time dependence of negative buoyancy and the subduction of continental lithosphere. Journal of Geodynamics 30, 539–555.
Rawlinson, N., Kennett, B.L.N., 2008. Teleseismic tomography of the upper mantle beneath the southern Lachlan Orogen, Australia. Physics of the Earth and Planetary Interiors 167, 84–97.
Rawlinson, N., Reading, A.M., Kennett, B.L.N., 2006. Lithospheric structure of Tasmania from a novel form of teleseismic tomography. Journal of Geophysical Research 111, B02301.
Rawlinson, N., Kennett, B.L.N., Vanacore, E., Glen, R.A., Fishwick, S., 2010. The structure of the upper mantle beneath the Delamerian and Lachlan orogens from simultaneous inversion of multiple teleseismic datasets. Gondwana Research 19 (3), 788–799.
Regenauer-Lieb, K., Yuen, D., Branlund, J., 2001. The initiation of subduction: criticality by addition of water? Science 294, 578–580.
Ren, Y., Shen, Y., 2008. Finite-frequency tomography in southeastern Tibet: evidence for the causal relation bentween mantle lithosphere delamination and the north-south-trending rifts. Journal of Geophysical Research 113, B10316.
Ren, Y., Stuart, G., Houseman, G., Dando, B., Ionescu, C., Hegedus, E., Radovanovic, S., Shen, Y., 2012. South Carpathian project working group. Earth and Planetary Science Letters 349–350, 139–152.
Richard, G., Iwamori, H., 2010. Stagnant slab, wet plumes and Cenozoic volcanism in East Asia. Physics of the Earth and Planetary Interiors 183, 280–287.
Ritsema, J., van Heijst, H., Woodhouse, J., 1999. Complex shear wave velocity structure imaged beneath Africa and Iceland. Science 286, 1925–1928.
Ritter, J., Jordan, M., Christensen, U., Achauer, U., 2001. A mantle plume below the Eifel volcanic fields, Germany. Earth and Planetary Science Letters 186, 7–14.
Rosenbaum, G., Gasparon, M., Lucente, F., Peccerillo, A., Miller, M., 2008. Kinematics of slab tear faults during subduction segmentation and implications for Italian magmatism. Tectonics 27. Available at: <http://dx.doi.org/10.1029/2007TC002143>.
Salah, M., Zhao, D., Lei, J., Abdelwahed, M., 2005. Crustal heterogeneity beneath southwest Japan estimated from direct and Moho-reflected waves. Tectonophysics 395, 1–17.
Savage, M., 1999. Seismic anisotropy and mantle deformation: what have we learned from shear wave splitting? Review of Geophysics 37 (1), 65–106.
Senshu, H., Maruyama, S., Rino, S., Santosh, M., 2009. Role of tonalite-trondhjemite-granite (TTG) crust subduction on the mechanism of supercontinent breakup. Gondwana Research 15, 433–442.
Shangguan, Z., Bai, C., Song, M., 2000. Mantle-derived magmatic gas releasing features at Rehai area, Tengchong county, Yunnan province, China. Science in China Series D: Earth Science 43 (2), 132–140.
Shemenda, A., 1993. Subduction of the lithosphere and back arc dynamics insights from physical modeling. Journal of Geophysical Research 98, 16167–16185.
Shen, X., Zhou, H., Kawakatsu, H., 2008. Mapping the upper mantle discontinuities beneath China with teleseismic receiver functions. Earth Planets Space 60, 713–719.

Shieh, S., Mao, H., Hemley, R., Ming, L., 1998. Decomposition of phase D in the lower mantle and the fate of dense hydrous silicates in subducting slabs. Earth and Planetary Science Letters 159, 13–23.
Sigloch, K., McQuarrie, N., Nolet, G., 2008. Two-stage subduction history under North America inferred from multiple-frequency tomography. Nature Geoscience 1, 458–462.
Silver, P.G., 1996. Seismic anisotropy beneath the continents: probing the depths of geology. Annual Review of Earth and Planetary Science 24, 385–432.
Simkin, T., Siebert, L., 1994. Volcanoes of the world. Geoscience Press, Washington D.C., p. 111.
Sleep, N.H., Richards, M.A., Hager, B.H., 1988. Onset of mantle plumes in the presence of preexisting convection. Journal of Geophysical Research 93, 7672–7689.
Song, Z., Zhang, G., Liu, J., Yin, J., Xue, Y., Song, X., 2011. Global earthquake catalog. Seismological press, Beijing, pp. 1–450.
Steinberger, B., Antretter, M., 2006. Conduit diameter and buoyant rising speed of mantle plumes: implications for the motion of hot spots and shape of plume conduits. Geochemistry Geophysics Geosystems 7. http://dx.doi.org/10.1029/2006GC001409.
Steinberger, B., Torsvik, T.H., 2012. A geodynamic model of plumes from the margins of Large Low Shear Velocity Provinces, Geochemistry Geophysics Geosystems 13, Q01W09.
Sun, A., Zhao, D., Ikeda, M., Chen, Y., Chen, Q., 2008. Seismic imaging of southwest Japan using P and PmP data: implications for arc magmatism and seismotectonics. Gondwana Research 14, 535–542.
Sun, C., Chen, Y., Gao, E., 2011. The crustal anisotropy and its geodynamical significance of the strong basin-range interaction zone beneath the east margin of Qinghai-Tibet plateau. Chinese Journal of Geophysics 54 (5), 1205–1214.
Tang, J., Liu, T., Jiang, Z., 1997. Preliminary observations of the Tianchi volcano area in Changbaishan Mountain by MT method. Seismology and Geology 19 (2), 164–170.
Tang, J., Deng, Q., Zhao, G., 2001. Electric conductivity and magma chamber at the Tianchi volcano area in Changbaishan Mountain. Seismology and Geology 23 (2), 191–200.
Tang, Y., Zhang, H., Ying, J., Zhang, J., Liu, X., 2008. Refertilization of ancient lithospheric mantle beneath the central North China Craton: evidence from petrology and geochemistry of peridotite xenoliths. Lithos 101, 435–452.
Tapponnier, P., Peltzer, G., Armijo, R., 1986. On the mechanics of the collision between India and Asia. In: Coward, M., Ries, A. (Eds.), Collision Tectonics, vol. 19, Geol. Soc. London Spec. Publ., 115–157.
Tatsumi, Y., Maruyama, S., Nohda, S., 1990. Mechanism of backarc opening in the Japan Sea: role of asthenospheric injection. Tectonophysics 181, 299–306.
Teng, J., Zhang, Z., Zhang, B., Yang, D., Wang, Z., Zhang, H., 1997. Geophysical fields and background of exceptional structure for deep latent mantle plume in Bohai Sea. Chinese Journal of Geophysics 40, 468–480.
Tian, Y., Zhao, D., 2012. P-wave tomography of the western United States: insight into the Yellowstone hotspot and the Juan de Fuca slab. Physics of the Earth and Planetary Interiors 200, 72–84.
Tian, Y., Zhao, D., Sun, R., Teng, J., 2009. Seismic imaging of the crust and upper mantle beneath the North China Craton. Physics of the Earth and Planetary Interiors 172, 169–182.
Tonegawa, T., Hirahara, K., Shibutani, T., Iwamori, H., Kanamori, H., Shiomi, K., 2008. Water flow to the mantle transition zone inferred from a receiver function image of the Pacific slab. Earth and Planetary Science Letters 274, 346–354.
Tong, P., Zhao, D., Yang, D., 2011. Tomography of the 1995 Kobe earthquake area: comparison of finite-frequency and ray approaches. Geophysical Journal International 187, 278–302.
Tong, P., Zhao, D., Yang, D., 2012. Tomography of the 2011 Iwaki earthquake (M 7.0) and Fukushima nuclear power plant area. Solid Earth 3, 43–51.
Turcotte, D.L., Schubert, G., 1982. Geodynamics, applications of continuum physics to geological problems. John Wiley and Sons press, New York, p. 44.
van der Hilst, R., de Hoop, M., 2005. Banana-doughnut kernels and mantle tomography. Geophysical Journal International 163, 956–961.
Vasco, D., Johnson, L., 1998. Whole Earth structure estimated from seismic arrival times. Journal of Geophysical Research 103, 2633–2671.
Wang, X., 2011. Temperature, pressure, and composition of the mantle source region for late Cenozoic basalts in Hainan island, Southeastern Asia: results of a young thermal mantle plume close to subduction zone? Journal of Petrology. http://dx.doi.org/10.1093/petrology/egr061.
Wang, C., Huangfu, G., 2004. Crustal structure in Tengchong volcano-geothermal area, western Yuannan, China. Tectonophysics 380, 69–87.
Wang, Y., Wen, L., 2007. Complex seismic anisotropy at the border of a very low velocity province at the base of the Earth's mantle. Journal of Geophysical Research 112, B09305.
Wang, J., Zhao, D., 2008. P-wave anisotropic tomography beneath Northeast Japan. Physics of the Earth and Planetary Interiors 170, 115–133.
Wang, J., Yin, A., Harrison, T., Grove, M., Zhang, Y., Xie, G., 2001. A tectonic model for Cenozoic igneous activities in the eastern Indo-Asian collision zone. Earth and Planetary Science Letters 188, 123–133.
Wang, C., Chan, W., Mooney, W., 2003a. Three-dimensional velocity structure of crust and upper mantle in southwestern China and its tectonic implications. Journal of Geophysical Research 108. http://dx.doi.org/10.1029/2002JB001973.
Wang, Y., Li, C., Wei, H., Shan, X., 2003b. Late Pliocene-recent tectonic setting for the Tianchi volcanic zone, Changbaishan Mountains, northeast China. Journal of Asian Earth Sciences 21, 1159–1170.
Wang, C., Flesch, L., Silver, P., Chang, L., Chan, W., 2008. Evidence for mechanically coupled lithosphere in central Asia and resulting implications. Geology 36 (5), 363–366.
Wei, H., Liu, G., Gill, J., 2013. Review of eruptive activity at Tianchi volcano, Changbaishan, northeast China: implications for possible future eruptions. Bulletin of Volcanology 75, 706, http://dx.doi.org/10.1007/s00445-013-0706-5.
Wessel, P., Smith, W., 1995. New version of the Generic Mapping Tools (GMT) version 3.0 released, EOS Trans. AGU 76, 329.
West, M., Gao, W., Grand, S., 2004. A simple approach to the joint inversion of seismic body and surface applied to the southwest U.S. Geophysical Research Letters 31, L15615.
Wolfe, C., Bjarnason, I., VanDecar, J., Solomon, S., 1997. Seismic structure of the Iceland mantle plume. Nature 385, 245–247.
Wu, J., Ming, Y., Zhang, H., Su, W., Liu, Y., 2005. Seismic activity at the Changbaishan Tianchi volcano in the Summer of 2002. Chinese Journal of Geophysics 48 (3), 621–628.
Wu, J., Ming, Y., Zhang, H., Liu, G., Fang, L., Su, W., Wang, W., 2007. Earthquake swarm activity in Changbaishan Tianchi volcano. Chinese Journal of Geophysics 50 (4), 1089–1096.
Wu, J., Gao, Y., Chen, Y., 2009. Shear-wave splitting in the crust beneath the southeast Capital area of North China. Journal of Seismology 13, 277–286.
Xia, S., Zhao, D., Qiu, X., Nakajima, J., Matsuzawa, T., Hasegawa, A., 2007. Mapping the crustal structure under active volcanoes in central Tohoku, Japan using P and PmP data. Geophysical Research Letters 34. http://dx.doi.org/10.1029/2007GL030026.
Xu, Y., Ma, J., Frey, F., Feigenson, M., Liu, J., 2005. Role of lithosphere-asthenosphere interaction in the genesis of Quaternary alkali and tholeiitic basalts from Datong, western North China Craton. Chemical Geology 224, 247–271.
Xu, Y., Yang, Q., Lan, J., Luo, Z., Huang, X., Shi, Y., Xie, L., 2012a. Temporal-spatial distribution and tectonic implications of the batholiths in the Gaoligong-Tengliang-Yingjiang area, western Yunnan: constraints from zircon U–Pb ages and Hf isotopes. Journal of Asian Earth Sciences 53, 151–175.
Xu, Y., Wei, J., Qiu, H., Zhang, H., Huang, X., 2012b. Opening and evolution of the South China Sea constrained by studies on volcanic rocks: preliminary results and a research design. Chinese Science Bulletin 2012, 57. http://dx.doi.org/10.1007/s11434-011-4921-1.
Xu, J., Liu, G., Wu, J., et al., 2012c. Recent unrest of Changbaishan volcano, northeast China: a precursor of a future eruption? Geophysical Research Letters. http://dx.doi.org/10.1029/2012GL052600.
Xue, M., Allen, R.A., 2007. The fate of the Juan de Fuca plate: implications for a Yellowstone plume head. Earth and Planetary Science Letters 264, 266–276.
Yan, Q., Shi, X., 2007. The Hainan mantle plume and the evolution of the South China Sea. Geological Journal of China Universities 13, 311–322.
Yang, T., Shen, Y., van der Lee, S., Solomon, S., Hung, S., 2006. Upper mantle structure beneath the Azores hotspot from finite-frequency seismic tomography. Earth and Planetary Science Letters 250, 11–26.
Yi, G., Yao, H., Zhu, J., van der Hilst, R., 2010. Lithospheric deformation of continental China from Rayleigh wave azimuthal anisotropy. Chinese Journal of Geophysics 53 (2), 256–268.
Yin, A., 2000. Mode of Cenozoic east-west extension in Tibet suggesting a common origin of rifts in Asia during the Indo-Asian collision. Journal of Geophysical Research 105, 21745–21759.
Yin, A., Harrison, T., 2000. Geological evolution of the Himalayan-Tibetan orogen. Annual Review of Earth and Planetary Sciences 28, 211–280.
Zhang, L., Tang, X., 1983. Subduction of the West Pacific Plate and deep-source seismic zone in Northeast China. Acta Geophysica Sinica 26, 331–340.
Zhang, C., Zhang, X., Zhao, J., Liu, B., Zhang, J., Yang, Z., Hai, Y., Sun, G., 2002. Crust-mantle structure of the Changbaishan Tianchi volcanic region and its vicinity: an exploratory study and inferences. Chinese Journal of Geophysics 45 (6), 862–871.
Zhang, H., Nakamura, E., Kobayashi, K., Zhang, J., Ying, J., Tang, Y., Niu, L., 2007. Transformation of subcontinental lithospheric mantle through deformation-enhanced peridotite-melt reaction: evidence from a highly fertile mantle xenolith from the North China Craton. International Geology Review 49, 658–679.
Zhang, G., Wu, Q., Pan, J., et al., 2013. Crustal thickness and Poisson's ratio under northeastern China using H-κ and CCP stacking methods. Chinese Journal of Geophysics.
Zhao, D., 2001. Seismic structure and origin of hotspots and mantle plumes. Earth and Planetary Science Letters 192, 251–265.
Zhao, D., 2004. Global tomographic images of mantle plumes and subducting slabs: insight into deep Earth dynamics. Physics of the Earth and Planetary Interiors 146, 3–34.
Zhao, D., 2007. Seismic images under 60 hotspots: search for mantle plumes. Gondwana Research 12, 335–355.
Zhao, D., 2009. Multiscale seismic tomography and mantle dynamics. Gondwana Reserch 15, 297–323.
Zhao, D., Liu, L., 2010. Deep structure and origin of active volcanoes in China. Geoscience Frontiers 1, 31–44.
Zhao, D., Hasegawa, A., Kanamori, H., 1994. Deep structure of Japan subduction zone as derived from local, regional, and teleseismic events. Journal of Geophysical Research 99, 22313–22329.
Zhao, D., Kanamori, H., Negishi, H., Wiens, D., 1996. Tomography of the source area of the 1995 Kobe earthquake: evidence for fluids at the hypocenter? Science 274, 1891–1894.

Zhao, D., Xu, Y., Wiens, D., Dorman, L., Hidebrand, J., Webb, S., 1997. Depth extent of the Lau back-arc spreading center and its relation to subducting processes. Science 278, 254–257.
Zhao, D., Lei, J., Tang, R., 2004. Origin of the Changbaishan intraplate volcanism in Northeast China: evidence from seismic tomography. Chinese Science Bulletin 49, 1401–1408.
Zhao, D., Todo, S., Lei, J., 2005. Local earthquake reflection tomography of the Landers aftershock areas. Earth and Planetary Science Letters 235, 623–631.
Zhao, C., Hua, R., Chen, K., 2006. Present-day magma chambers in Tengchong volcano area inferred from relative geothermal gradient. Acta Petrologica Sinica 22 (6), 1517–1528.
Zhao, D., Maruyama, S., Omori, S., 2007a. Mantle dynamics of Western Pacific and East Asia: insight from seismic tomography and mineral physics. Gondwana Research 11, 120–131.
Zhao, L., Zheng, T., Chen, L., Tang, Q., 2007b. Shear wave splitting in eastern and central China: implications for upper mantle deformation beneath continental margin. Physics of the Earth and Planetary Interiors 162, 73–84.
Zhao, Y., Fan, Q., Bai, Z., Sun, Q., Li, N., Sui, J., Du, X., 2008. Preliminary study on Quaternary volcanoes in the Halaha River and Chaoer River area in Daxing' an Mountain range. Acta Petrologica Sinica 24 (11), 2569–2575.
Zhao, D., Tian, Y., Lei, J., Liu, L., Zheng, S., 2009a. Seismic image and origin of the Changbaishan intraplate volcano in East Asia: role of big mantle wedge above the stagnant Pacific slab. Physics of the Earth and Planetary Interiors 173, 197–206.
Zhao, L., Allen, R., Zheng, T., Hung, S., 2009b. Reactivation of an Archean craton: constraints from P- and S-wave tomography in North China. Geophysical Research Letters 36, L17306.
Zhao, C., Ran, H., Chen, K., 2011. Present-day temperatures of magma chambers in the crust beneath Tengchong volcanic field, southwestern China: estimation from carbon isotopic fractionation between CO_2 and CH_4 of free gases escaped from thermal springs. Acta Petrologica Sinica 27 (10), 2883–2897.
Zhao, D., Huang, Z., Umino, N., Hasegawa, A., Kanamori, H., 2011a. Structural heterogeneities in the megathrust zone and mechanism of the 2011 Tohoku-oki earthquake (Mw 9.0). Geophysical Research Letters 38, L17308.
Zhao, D., Yu, S., Ohtani, E., 2011b. East Asia: seismotectonics, magmatism and mantle dynamics. Journal of Asian Earth Sciences 40, 689–709.
Zhao, D., Yanada, T., Hasegawa, A., Umino, N., Wei, W., 2012a. Imaging the subducting slabs and mantle upwelling under the Japan Islands. Geophysical Journal International 190, 816–828.
Zhao, D., Yamamoto, Y., Yanada, T., 2013. Global mantle heterogeneity and its influence on teleseismic regional tomography. Gondwana Research 23, 595–616.
Zhao, C., Ran, H., Wang, Y., 2012c. Present-day mantle-derived helium release in the Tengchong volcanic field, southwest China: implications for tectonics and magmatism. Acta Petrologica Sinica 28 (4), 1189–1204.
Zhao, L., Zheng, T., Lu, G., 2012b. Distinct upper mantle deformation of cratons in response to subduction: Constraints from SKS wave splitting measurements in eastern China. Gondwana Research. Available at: <http://dx.doi.org/10.1016/j.gr.2012.04.007>.
Zheng, X., Ouyang, B., Zhang, D., et al., 2009. Technical system construction of Data Backup Center for China seismograph network and the data support to researches on the Wenchuan earthquake. Chinese Journal of Geophysics 52 (5), 1412–1417.
Zheng, X., Yao, Z., Liang, J., Zheng, J., 2010. The role played and opportunities provided by IGP DMC of China National Seismic Network in Wenchuan Earthquake Disaster Relief and Researches. Bulletin of the Seismological Society of America 100, 2866–2872.
Zhou, M., Robinson, P., Wang, C., Zhao, J., Yan, D., Gao, J., Malpas, J., 2011. Heterogeneous mantle source and magma differentiation of quaternary arc-like volcanic rocks from Tengchong, SE margin of the Tibetan Plateau. Contributions to Mineralogy and Petrology. http://dx.doi.org/10.1007/s00410-011-0702-8.
Zhu, B., Mao, C., Lugmair, G., Macdougall, J., 1983. Isotopic and geochemical evidence for the origin of Plio-Pleistocene volcanic rocks near the Indo-Eurasian collisional margin at Tengchong, China. Earth and Planetary Science Letters 65, 263–275.
Zhu, R., Chen, L., Wu, F., Liu, J., 2011. Timing, scale and mechanism of the destruction of the North China Craton. Science China Earth Sciences 54, 789–797.
Zindler, A., Hart, S., 1986. Chemical geodynamics. Annual Review of Earth and Planetary Sciences 14, 463–471.
Zou, H., Fan, Q., 2010. U-Th isotopes in Hainan basalts: Implications for sub-asthenospheric origin of EM2 mantle endmember and the dynamics of melting beneath Hainan Island. Lithos 116, 145–152.
Zou, H., Fan, Q., Yao, Y., 2008. U-Th systematics of dispersed young volcanoes in NE China: asthenosphere upwelling caused by piling up and upward thickening of stagnant Pacific slab. Chemical Geology 255, 134–142.
Zou, H., Fan, Q., Schmitt, A., Sui, J., 2010a. U-Th dating of zircons from Holocene potassi andestites (Maanshan volcano, Tengchong, SE Tibetan plateau) by depth profiling: time scales and nature of magma storage. Lithos 118, 202–210.
Zou, H., Fan, Q., Zhang, H., 2010b. Rapid development of the great Millennium eruption of Changbaishan (Tianchi) Volcano, China/North Korea: evidence from U–Th zircon dating. Lithos 119, 289–296.